JACS
JOURNAL OF THE AMERICAN CHEMICAL SOCIETY

ARTICLE

pubs.acs.org/JACS

Neomycin−Neomycin Dimer: An All-Carbohydrate Scaffold with High Affinity for AT-Rich DNA Duplexes

Sunil Kumar, Liang Xue,# and Dev P. Arya*

Laboratory of Medicinal Chemistry, Department of Chemistry, Clemson University, Clemson, South Carolina 29634, United States

Supporting Information

ABSTRACT: A dimeric neomycin−neomycin conjugate **3** with a flexible linker, 2,2′-(ethylenedioxy)bis(ethylamine), has been synthesized and characterized. Dimer **3** can selectively bind to AT-rich DNA duplexes with high affinity. Biophysical studies have been performed between **3** and different nucleic acids with varying base composition and conformation by using ITC (isothermal calorimetry), CD (circular dichroism), FID (fluorescent intercalator displacement), and UV (ultraviolet) thermal denaturation experiments. A few conclusions can be drawn from this study: (1) FID assay with **3** and polynucleotides demonstrates the preference of **3** toward AT-rich sequences over GC-rich sequences. (2) FID assay and UV thermal denaturation experiments show that **3** has a higher affinity for the poly(dA)·poly(dT) DNA duplex than for the poly(dA)·2poly(dT) DNA triplex. Contrary to neomycin, **3** destabilizes poly(dA)·2poly(dT) triplex but stabilizes poly(dA)·poly(dT) duplex, suggesting the major groove as the binding site. (3) UV thermal denaturation studies and ITC experiments show that **3** stabilizes continuous AT-tract DNA better than DNA duplexes with alternating AT bases. (4) CD and FID titration studies show a DNA binding site size of 10−12 base pairs/drug, depending upon the structure/sequence of the duplex for AT-rich DNA duplexes. (5) FID and ITC titration between **3** and an intramolecular DNA duplex [d(5′-A_{12}-x-T_{12}-3′), x = hexaethylene glycol linker] results in a binding stoichiometry of 1:1 with a binding constant ∼10^8 M^{-1} at 100 mM KCl. (6) FID assay using **3** and 512 hairpin DNA sequences that vary in their AT base content and placement also show a higher binding selectivity of **3** toward continuous AT-rich than toward DNA duplexes with alternate AT base pairs. (7) Salt-dependent studies indicate the formation of three ion pairs during binding of the DNA duplex d[5′-A_{12}-x-T_{12}-3′] and **3**. (8) ITC-derived binding constants between **3** and DNA duplexes have the following order: AT continuous, d[5′-$G_3A_5T_5C_3$-3′] > AT alternate, d[5′-$G_3(AT)_5C_3$-3′] > GC-rich d[5′-$A_3G_5C_5T_3$-3′]. (9) **3** binds to the AT-tract-containing DNA duplex (B* DNA, d[5′-$G_3A_5T_5C_3$-3′]) with 1 order of magnitude higher affinity than to a DNA duplex with alternating AT base pairs (B DNA, d[5′-$G_3(AT)_5C_3$-3′]) and with almost 3 orders of magnitude higher affinity than a GC-rich DNA (A-form, d[5′-$A_3G_5C_5T_3$-3′]).

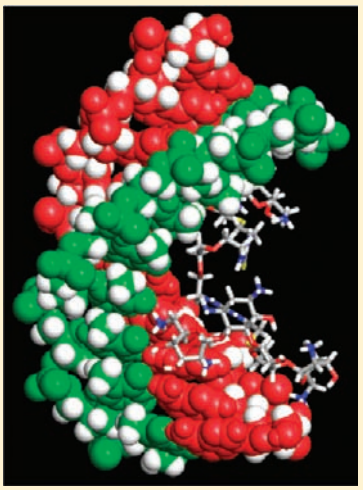

INTRODUCTION

Targeting nucleic acids by small molecules has been of long-standing interest to scientists due to the challenges inherent in macromolecular recognition and also because of the fundamental therapeutic potential of the exercise. Exploration of small molecules binding to duplex DNA has become an active research area, as the complexes formed by small molecules and DNA can alter natural gene expression and consequently regulate cell growth.[1,2] The DNA−small molecule interactions are dictated by both covalent and noncovalent binding modes. A majority of the noncovalent DNA−small molecule binding interactions take place via two modes:[3] intercalation[3,4] and groove binding.[1,5,6] The resulting DNA−drug complex is usually stabilized by noncovalent interactions, such as hydrogen bonds, van der Waals, and electrostatic interactions. Considerable efforts have been invested to develop sequence-specific DNA binding ligands in the past several decades. Dervan and co-workers have developed polyamides[7,8] derived from natural product distamycin,[9] which have expanded the list of sequence-selective DNA binding ligands.[10] Most DNA binding ligands are planar heterocycles that intercalate between the DNA bases or stack in the minor groove. However, nonplanar molecules that bind to DNA are virtually nonexistent. Recognition of duplex DNA and other nucleic acids by carbohydrate-containing molecules has come to the forefront in recent years.[11] A number of DNA binding agents with carbohydrate domains, such as bleomycin,[12] rebeccamycin,[13] gemtuzumab ozogamicin,[11,14] and chromomycin[15] have been studied. The role of the carbohydrate moiety in these DNA binders has been investigated, and a recent investigation suggests that carbohydrate moieties appear responsible for drug targeting.[16] A number of DNA binding natural products have been shown to contain carbohydrate binding domains.[11] However, reports on DNA duplex binding ligands based solely on carbohydrate scaffolds are nonexistent. Previous studies reveal that polysaccharides with stereo- and spatial chemical constraints may have

Received: September 8, 2010
Published: April 27, 2011

dx.doi.org/10.1021/ja108118v | J. Am. Chem. Soc. 2011, 133, 7361–7375

the potential to specifically recognize DNA sequences, although these studies also included planar moieties in the DNA binding domains.[17−19] A dimeric calicheamicin containing a planar iodophenyl moeity showed a much higher affinity ($K_d = 10^{-9}$ M) with TCCT tract(s)[18] in a DNA duplex than that of the monomeric calicheamicin ($K_d = 10^{-6}$ M).[18,19]

Aminoglycosides are aminosugars linked through glycosidic linkages that bind to eubacterial RNA and have been effectively used as antibacterial antibiotics for almost 60 years.[20,21] Aminoglycosides have been known to target different structures of RNA such as 5′-untranslated region of thymidylate synthase mRNA,[22] rev response element and the transactivating response element RNA motifs of HIV-1,[23,24] group I introns,[25] ribonuclease P RNA,[26] hairpin ribozyme,[27] and hammerhead ribozyme.[28] We have previously reported that aminosugars can act as major groove binding scaffolds for DNA triplexes.[29] These findings supplemented the various RNA binding properties of aminosugars.[30−33] Our findings showed that neomycin (and other aminoglycosides) can stabilize DNA[34−38] and RNA triplexes,[29,35] DNA/RNA hybrid duplexes/triplexes,[39,40] poly (A),[41] and even DNA quadruplex.[42] The binding properties of aminoglycosides have been further expanded by conjugating them with intercalators,[43] with minor groove binders,[44−46] and with oligonucleotides,[47−49] because neomycin also assists in lipid-mediated delivery of oligonucleotides.[50] Neomycin fits better in the narrower A-form major groove[51] but does not have a good shape and potential complementarity to the wider major groove of B-form DNA. The larger size of the B/B*-form major groove prompted us to investigate dimeric aminoglycosides[52,53] that could show a better shape and potential complementarity to the major groove of B/B*-form DNA. B*-form DNA refers to AT-rich DNA sequences that contain long A-tracts that lead to an unusually narrow minor groove and high base-pair propeller twist.[54] Herein, we report that a dimeric aminoglycoside with a flexible thioether linker has been synthesized[52,55] and shows a high binding affinity to duplex DNA. A neomycin−neomycin conjugate **3** has been synthesized by coupling neomycin amine **1** (2 equiv) with 2,2′-(ethylenedioxy)bis(ethylisothiocyanate) (Scheme 1). We report that dimer **3** binds long stretches of AT-rich DNA double helices with remarkably high affinity. To the best of our knowledge, this report outlines the first example of an all-carbohydrate pharmacophore that contains no planar moieties yet binds to DNA duplexes with high affinities and with structure and sequence-selectivity.

EXPERIMENTAL PROCEDURES

Materials. All of the chemicals were purchased from commercial suppliers and used without further purification. Neomycin B trisulfate was purchased from MP Biomedicals (Solon, Ohio). Di-*tert*-butyl dicarbonate (Boc anhydride) was purchased from Advanced ChemTech (Louisville, KY). SC (sodium cacodylate), EDTA (ethylenediamine tetraacetic acid), KCl, and sodium phosphate (mono and di) salts were purchased from Fisher Scientific. 2,2′-(Ethylenedioxy)bis(ethylamine) and DMAP (4-(dimethylamino)pyridine) were purchased from Acros organics. TCDP (1,1′-thiocarbonyldi-2(1*H*)-pyridone), TPS-Cl (2,4,6-triisopropylbenzenesulfonyl chloride), and 4 M HCl/dioxane were purchased from Sigma Aldrich. Silica gel for flash column chromatography was purchased from Sorbent Technologies (Atlanta, GA) as silica gel standard grade (particle size = 40−63 μm). All solvents were purchased from VWR. Reaction solvents were distilled over calcium hydride [pyridine, DCM (dichloromethane)]. EtOH (ethanol) was first distilled with sodium metal and then redistilled over magnesium turnings. Reactions were carried out under N_2 using dry solvent, unless otherwise noted.

Instrumentation. ^{1}H NMR spectra were collected on a Bruker 500 MHz FT-NMR spectrometer. MS (MALDI-TOF) spectra were collected using a Bruker Omniflex MALDI-TOF mass spectrometer. All UV spectra were recorded on a Cary 100 Bio UV/vis spectrophotometer equipped with a thermoelectrically controlled 12-cell holder. Quartz cells with a 1 cm path length were used for all the absorbance studies. Spectrophotometer stability and λ alignment were checked prior to initiation of each melting point experiment. Isothermal titration calorimetric measurements were performed on a MicroCal VP-ITC (MicroCal, Inc. Northampton, MA). All CD experiments were conducted at 20 °C on a JASCO J-810 spectropolarimeter equipped with a thermoelectrically controlled cell holder. A quartz cell with a 1 cm path length was used in the CD studies. Fluorescence spectra were measured on a Photon Technology International instrument (Lawrenceville, NJ). The fluorescence measurements of 96-well plates were carried out on a Genios Multi-Detection Microplate Reader, TECAN with Magellan software.

Nucleic Acids. Homopolynucleotides were purchased from GE Healthcare (Picataway, NJ). Native DNAs were purchased from Sigma Aldrich. The concentrations of the polymer solutions were determined by UV spectroscopy, using the following molar extinction coefficients: $\varepsilon_{265} = 9000\ M^{-1}\ cm^{-1}$ base^{-1} for poly(dT), $\varepsilon_{260} = 6000\ M^{-1}\ cm^{-1}\ bp^{-1}$ for poly(dA)·poly(dT), $\varepsilon_{260} = 7600\ M^{-1}\ cm^{-1}\ bp^{-1}$ for poly(dA·dT)$_2$, $\varepsilon_{253} = 7400$ for poly(dG)·poly(dC), $\varepsilon_{260} = 12\,824\ M^{-1}\ cm^{-1}\ bp^{-1}$ for DNA from *Calf thymus* (42%, G+C bases), $\varepsilon_{260} = 12\,476\ M^{-1}\ cm^{-1}\ bp^{-1}$ for DNA from *Clostridium perfringens* (31%, G+C bases), $\varepsilon_{260} = 13\,846\ M^{-1}\ cm^{-1}\ bp^{-1}$ for DNA from *Micrococcus lysodeikticus* (72%, G+C bases). The 12-mer duplex d[5′-A_{12}-x-T_{12}-3′] oligonucleotide was synthesized on Applied Biosystem 8890 using standard phosphoramidite chemistry and purified by HPLC on a Gen-Pak FAX (4.6 × 100 mm) ion exchange column, eluting with buffer A (25 mM Tris·HCl, 1 mM EDTA, 10% CH_3CN, pH 8.0) from 98% to 50% and buffer B (25 mM Tris·HCl, 1 mM EDTA, 1 M $NaClO_4$, 10% CH_3CN, pH 8.0) from 2% to 50% in 15 min.

The intramolecular triplex d[5′-A_{12}-x-T_{12}-x-T_{12}-3′] was synthesized using an Expedite Nucleic Acid Synthesis System (8909) with standard phosphoramidite chemistry. The oligomer was purified on an anion exchange HPLC column (Water Gen-Pak FAX, 4.6 × 100 mm) with a Tris·HCl buffer system. Buffer A: 25 mM Tris·HCl, 1 mM EDTA, and 10% MeCN (v/v%); buffer B: buffer A + 1 M NaCl. Conditions: 2−60% buffer B over buffer A during 0−16 min at a flow rate of 0.75 mL/min. Hairpin deoxyoligonucleotides were purchased from Eurofins MWG/Operon (Huntsville, AL) as 50 μM/strand solutions in 200 μL water and stored as stock solutions at −20 °C. All other oligonucleotides were purchased from IDT DNA (Coralville, IA). The concentrations of all the oligonucleotides were determined by UV using the following extinction coefficients (in units of mol of nucleotide/$L^{-1}\ cm^{-1}$): $\varepsilon_{260} = 163\,500$ for d[5′-A_8T_8-3′], $\varepsilon_{260} = 160\,700$ for d[5′-GA_7T_7C-3′], $\varepsilon_{260} = 157\,900$ for d[5′-$G_2A_6T_6C_2$-3′], $\varepsilon_{260} = 155{,}100$ for d d[5′-$G_3A_5T_5C_3$-3′], $\varepsilon_{260} = 152\,300$ for d [5′-$G_4A_4T_4C_4$-3′], $\varepsilon_{260} = 147\,300$ for d [5′-$G_5A_3T_3C_5$-3′], $\varepsilon_{260} = 145\,000$ for d[5′-$G_6A_2T_2C_6$-3′], $\varepsilon_{260} = 259\,844$ for d[5′-A_{12}-x-T_{12}-3′], $\varepsilon_{260} = 341\,100$ for d[5′-A_{12}-x-T_{12}-x-T_{12}-3′], $\varepsilon_{260} = 159\,266$ for d[5′-$G_3(AT)_5C_3$-3′], $\varepsilon_{260} = 159\,266$ for d[5′-GGGAATTAATTATCCC-3′], $\varepsilon_{260} = 159\,266$ for d[5′-GGGATAATTAATTCCC-3′], $\varepsilon_{260} = 176{,}968$ for d[5′-GGGATAATAAAAACCC-3′], $\varepsilon_{260} = 141\,563$ for d[5′-GGGTTTTTATTATCCC-3′], $\varepsilon_{260} = 165\,166$ for d[5′-GGGATATATAAATCCC-3′], $\varepsilon_{260} = 153{,}365$ for d[5′-GGGATTTATATATCCC-3′], $\varepsilon_{260} = 269\,990$ for d[5′-AAGGG-$(AT)_{12}$GGGAA-3′], $\varepsilon_{260} = 178\,970$ for d[5′-TTCCC$(TA)_{12}$CCCTT-3′], $\varepsilon_{260} = 178\,970$ for d[5′-AAGAGGAGAGAAGAGAGGAGAA-3′], $\varepsilon_{260} = 159\,844$ for d[3′-TTCTCCTCTCTTCTCTCCTCTT-5′], $\varepsilon_{260} = 283\,233$ for d[5′-AAGGG$(A)_{12}$GGGAA-3′], $\varepsilon_{260} = 157\,343$ for

d[5′-TTCCC(T)$_{12}$CCCTT-3′]. The term r_{db} refers to molar ratio of drug to base pair.

UV Spectroscopy. The UV thermal denaturation samples (1 mL) were prepared by mixing DNA (1 μM/duplex for oligonucleotides, 15 μM/bp for polymer duplexes, or 15 μM/triplet for polymer triplexes) in 100 or 150 mM KCl, 10 mM SC, 0.5 mM EDTA, pH 6.8. In case of oligonucleotides, prior to UV thermal denaturation experiments, the samples were heated to 95 °C for 5 min and then slowly cooled to room temperature and incubated at 4 °C for 16 h. In the polynucleotide experiments, the samples were heated to 95 °C followed by annealing to room temperature at a rate of 0.2 °C/min. The UV thermal denaturation spectra of the samples in 1 cm path length quartz cuvettes was recorded at 260, 280, and 284 nm as a function of temperature (10−95 °C, heating rate: 0.2 °C/min). First derivative plots were used to determine the dentauration temperature.

Circular Dichroism Spectroscopy (CD). Small aliquots (0.6−5.0 μL) of a concentrated **3** solution (0.5 mM or 1 mM) were added to a solution (2 mL, 100 mM KCl, 10 mM SC, 0.5 mM EDTA, pH 6.8) of DNA [poly(dA)·poly(dT) (50 μM/bp) or poly(dA·dT)$_2$ (50 μM/bp) and 4 μM/duplex for oligonucleotide], inverted twice, and incubated for 5 min at 20 °C. The CD spectra were then recorded as an average of three scans from 200 to 350 nm and data recorded in 0.1 nm increments with an averaging time of 2 s.

Isothermal Titration Calorimetry (ITC). In a typical experiment, an aliquot (9 μL) of **3** (125 μM in 100 mM KCl, 10 mM SC, 0.5 mM EDTA, pH 6.8) was injected at 25 °C into an isothermal sample chamber containing an oligonucleotide duplex solution (1.42 mL, 4 μM/duplex in 100 mM KCl, 10 mM SC, 0.5 mM EDTA, pH 6.8) via a 296 μL rotary syringe (300 rpm). The interval time between each injection was 300 s, and the duration time of each injection was 10 s. The initial delay prior to the first injection was 60 s. Injection of **3** at the same concentration into a buffer solution at 25 °C was used as a blank. Each injection generated a heat burst curve (microcalories per second). The area under each heat burst curve was determined by integration using the Origin (version 5.0, MicroCal, Inc. Northampton, MA) software to obtain a measure of the heat associated with that injection. The heat associated with each drug−buffer injection was subtracted from the corresponding heat associated with each drug−DNA injection to yield the heat of drug binding for that injection. The final corrected injection heats were plotted as a function of molar ratio ([drug]/[DNA]) and fitted with the one binding site model or with the two independent binding site model.

Fluorescent Intercalator Displacement Assay (FID). FID titrations for oligomeric DNA duplexes were carried out in a quartz cuvette. A thiazole orange (TO) solution (0.5 equiv/base pair, 2 mL) in sodium cacodylate buffer (100 mM KCl, 10 mM SC, 0.5 mM EDTA, pH 6.8) was prepared, and the fluorescence of this solution was measured (Ex: 504 nm and Em: 520−600 nm). An oligomeric duplex solution d[5′-A$_{12}$-x-T$_{12}$-3′] or d[5′-A$_{30}$.T$_{30}$-3′] was added into the TO solution to make a 1 μM/strand final concentration. The fluorescence of the mixture was measured again and normalized to 100% relative fluorescence. An aliquot of the stock solution of **3** (5 μM to 200 μM) was added into the mixture, and the fluorescence was measured after incubation for 5 min at 20 °C. The addition of **3** was continued until the fluorescence reached saturation. For all titrations, the final concentrations were corrected for dilution (less than 5% of the total volume).

FID assays for polymeric DNA were carried out in a 96-well plate. A solution containing polynucleotide (0.88 μM/bp) and TO was prepared by incubating the two for 30 min in buffer (100 mM KCl, 10 mM SC, 0.5 mM EDTA, pH 6.8) prior to the measurements. Each well of the 96-well plate (flat bottom, black) was loaded with polynucleotide solution (200 μL). A small aliquot of the stock solution of **3** (5 μM to 200 μM) or neomycin (50 μM to 25 mM) was added into each well to make a desired concentration of **3**, and the fluorescence was measured in triplicate after incubation for 5 min. Fluorescence readings are reported as percentage fluorescence relative to control wells. The reference fluorescence is defined as such: [TO+DNA] gives 100% fluorescence and [TO] only gives 0% fluorescence).

Ethidium Bromide Displacement Titration for Determining the Apparent DNA Binding Site Size. The binding stoichiometries of poly(dA)·poly(dT) and poly(dA·dT)$_2$ with **3** were determined by ethidium bromide displacement titration. A solution (100 mM KCl, 10 mM SC, 0.5 mM EDTA, pH 6.8) of the polymer [poly(dA)·poly(dT) or poly(dA·dT)$_2$, 10 μM/bp) saturated with EtBr (5 μM) was prepared. In a fluorescence quartz cuvette, small aliquots of the stock solution of **3** (100 μM to 1 mM) were added into the premixed DNA−EtBr solution (2 mL). The fluorescence was recorded after each addition until no more changes in fluorescence were observed. The percentage change of the fluorescence was then plotted against the ratio of drug to base pair.

Thiazole Orange (TO) FID Assay for 512-Member Deoxyoligonucleotide Library. Prior to use, each hairpin deoxyoligonucleotides was diluted to 40 μM/strand in buffer (100 mM KCl, 10 mM SC, 0.5 mM EDTA, pH 6.8) and stored at 4 °C. Each well plate was heated to 95 °C for 5 min, slowly cooled down to r.t., and stored at 4 °C for 16 h. Each well of a 96-well plate (flat bottom, black) was loaded with a mixture solution (200 μL) containing DNA (1 μM/strand) and TO (6 μM) in a buffer (100 mM KCl, 10 mM SC, 0.5 mM EDTA, pH 6.8). After incubation at 25 °C for 30 min, the fluorescence of each well was recorded (average of 10 readings, Ex: 495 nm and Em: 535 nm). Afterwords, 2 μL of **3** solution was added to each well from a stock solution (100 μM), and the solution was mixed thoroughly in each well before recording the fluorescence. All experiments were carried out in duplicate. The fluorescence readings with no ligand and with no DNA are defined as 100% and 0% fluorescence, respectively. Fluorescence readings are reported as percentage fluorescence relative to the control wells. The fluorescence plate reader shows a variability of ±10%.

2,2′-(Ethylenedioxy)bis(ethylisothiocyanate) (2). In a 25 mL round-bottom flask, 2,2′-(ethylenedioxy)bis(ethylamine) (13.8 mg, 0.135 mmol) was dissolved in 10 mL of anhydrous CH_2Cl_2 under a N_2 atmosphere. 1,1′-Thiocarbonyldi-2(1*H*)-pyridone (47.6 mg, 2.2 equiv) was added into the flask and stirred for 4 h at room temperature. The progress of the reaction was monitored by TLC. Flash chromatography of the residue (CH_2Cl_2) yielded the desired product as colorless oil (20.4 mg, 94%). R_f = 0.5 (silica gel, CH_2Cl_2); IR (cm^{-1}): 3350, 2950, 2920, 2100 (NCS), 1520, 1250, 1050; ^{1}H NMR (300 MHz, $CDCl_3$) δ 3.67−3.75 (m, 12H); ^{13}C NMR (125 MHz, $CDCl_3$) δ 132.6, 70.9, 69.4, 45.4; MS (EI) calcd For $C_8H_{12}N_2O_2S_2^+$ (M^+) 232.0340, found 232.0345. Anal. Calcd for $C_8H_{12}N_2O_2S_2$: C, 41.36; H, 5.21; N, 12.06. Found: C, 41.71; H, 5.32; N, 11.98.

N-Boc Dimer (3a). In a 25 mL round-bottom flask, 2,2′-(ethylenedioxy)bis(ethylisothiocyante) (1.623 mg, 0.007 mmol) was dissolved in 5.0 mL of anhydrous pyridine under N_2. Neomycin amine **1** (17.8 mg, 0.014 mmol, 2 equiv) and a catalytic amount of 4-(dimethylamino)pyridine were added to the flask and stirred at room temperature overnight. The reaction mixture was then concentrated. Flash chromatography of the residue (6% v/v CH_3OH in CH_2Cl_2) yielded the desired product as a white solid (18.5 mg, 95%): R_f = 0.6 (silica gel, 10% v/v CH_3OH in CH_2Cl_2); IR (cm^{-1}): 3375 (OH), 2930, 2870, 2150 (C═S), 1691, 1510. ^{1}H NMR (500 MHz, CD_3COCD_3): δ 7.52 (s, 2 H, (S═C-N*H*-CH$_2$-CH$_2$-O)), 7.30 (s, 2 H, C$_{5III}$-CH$_2$-CH$_2$-N*H*-C═S), 6.43 (t, 2H, J = 5 Hz, NH$_{6IV}$), 6.25−6.28 (m, 2H, NH$_{1I}$), 6.22 (d, 2H, J = 9 Hz, NH$_{6II}$), 6.08−6.15 (m, 4H, NH$_{3I}$ and NH$_{2IV}$), 5.95 (s, 2H, NH$_{2II}$), 5.21 (s, 2H, H$_{1II}$), 5.17 (d, 2H, J = 2 Hz, H$_{1III}$), 5.05 (d, 2H, J = 4.5 Hz, OH$_{4IV}$), 5.02 (s, 2H, H$_{1IV}$), 4.78 (s, 2H, OH$_{6I}$), 4.57 (s, 2H, OH$_{4II}$), 4.45−4.54 (m, 6H, OH), 4.35 (s, 2H, H$_{4III}$), 4.25−4.28 (m, 2H, H$_{2III}$), 4.23−4.24 (m, 4H, H$_{3III}$ and H$_{5IV}$ or H$_{3IV}$), 4.17−4.21 (m, 2H, H$_{3IV}$ or H$_{5IV}$), 4.04 (s, 2H, H$_{4IV}$), 3.90 (t, 2H, J = 7 Hz, H$_{2IV}$), 3.68−3.80 (m, 4H, H$_{5II}$ and H$_{5I}$), 3.62−3.66 (m, 12 H, O-CH$_2$-CH$_2$-O,

Scheme 1. Synthesis of Conjugate 3[a]

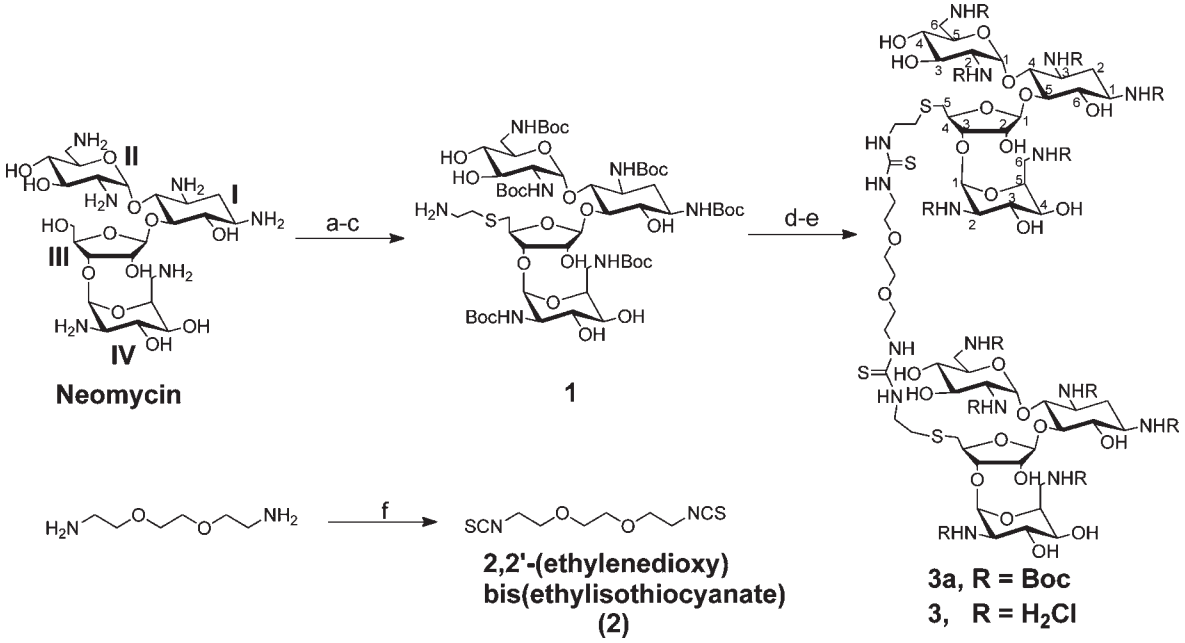

[a] Reagents and conditions: (a) $(Boc)_2O$, DMF, H_2O, Et_3N, 60°C, 5 h, 60%. (b) TPS-Cl, pyridine, r.t., 40 h, 50%. (c) $HSCH_2CH_2NH_2 \cdot HCl$, EtOH, EtONa, r.t., 12 h, 60%. (d) **2**, pyridine, DMAP, r.t., 12 h, 95%. (e) 4 M HCl/dioxane, $HSCH_2CH_2SH$, r.t., 5 min, 73%. (f) TCDP, dry DCM, r.t., 4 h, 94%.

linker protons), 3.55−3.61 (m, 12H, H_{6I}, H_{4I}, H_{3I}, H_{5III}, and H_{2II}), 3.40−3.52 (m, 4H, H_{3II} and H_{1I}), 3.15−3.30 (m, 10H, H_{4II}, H_{6IV}, and H_{6II}), 2.97−3.05 (m, 4H, C_{5III}-CH_2-CH_2-S), 2.23−2.35 (m, 2H, H_{2Ieq}), 1.66−1.75 (m, 2H, H_{2Iax}), 1.26−1.60 (m, 108 H, Boc protons); ^{13}C NMR (125 MHz, CD_3COCD_3): δ 167.9 (C═S), 157.6−156.4 (6 × Boc, C═O), 110.2 (C_{1III}), 100.8 (C_{1IV}), 98.9 (C_{1II}), 86.5 (C_{4I}), 82.1 (C_{3III}), 81.6 (C_{4III}), 81.6 (C_{6I}), 79.3−79.0 (6 × Boc, C_q), 74.3 (C_{3II}), 73.1 (C_{2III}), 72.9 (C_{4II}), 71.6 (C_{3IV} or C_{5IV}), 71.4 (C_{3IV} or C_{5IV}), 70.3 (C_{5II}), 69.9 (OCH_2CH_2O, linker), 69.3 (OCH_2CH_2O, linker), 67.7 (C_{5III}S-CH_2-CH_2-NH), 67.4 (C_{5III}-S-CH_2-CH_2-NH), 66.2 (C_{2II}), 56.0 (OCH_2CH_2NH, linker), 54.6 (C_{1I}), 52.5 (C_{3I}), 50.9 (C_{2IV}), 43.9 (C_{6II}), 41.9 (C_{6IV}), 40.0 (C_{5III}), 38.8, 32.3 (C_{2I}), 24.5−22.4 (6 × Boc, $(CH_3)_3$). MS MALDI-TOF calcd for $C_{118}H_{210}N_{16}O_{50}S_4$ ($M + Na^+$), 2804.26, obsd: 2804.694. Anal. Calcd for $C_{118}H_{210}N_{16}O_{50}S_4$: C, 50.96; H, 7.61; N, 8.06. Found: C, 51.28; H, 7.75; N, 7.90.

Dimer 3. **3a** (18.5 mg) was dissolved in dioxane (1.0 mL). 1,2-Ethanedithiol (3.0 μL) and 4 M HCl/dioxane (1.0 mL) were added into the mixture and swirled for 5 min by hand. A white solid precipitated during the reaction. Further precipitation was induced by adding ether and hexane (1 mL each). The precipitate was recovered by centrifugation and washed twice with ether (1.0 mL) and hexane (1.0 mL). The resulting solid was redissolved in DI water and lyophilized to dryness to yield the desired product as a white solid (9.79 mg, 73%): IR (cm^{-1}) 3385 (broad), 2100 (C═S), 1640, 1130; ^1H NMR (500 MHz, D_2O) δ 6.00−6.04 (m, 2H, H_{1II}), 5.82 (d, 2H, J = 3.5 Hz, OH), 5.36−5.39 (m, 2H, H_{1III}), 5.24 (s, 2H, H_{1IV}), 5.21 (s, 2H, OH), 4.43−4.45 (m, 2H, H_{4III}), 4.36−4.40 (m, 2H, H_{2III}), 4.21−4.29 (m, 4H, H_{5IV} or H_{3IV}, H_{3III}), 4.08−4.17 (m, 4H, H_{5IV} or H_{3IV} and H_{4I}), 3.90−3.98 (m, 4H, H_{3II} and H_{5II}), 3.80−3.87 (6H, H_{4IV}, H_{5I}, and H_{6I}), 3.56−3.75 (m, 12H, linker protons), 3.45−3.51 (m, 8H, H_{2II}, H_{2IV}, H_{4II}, and H_{3I}), 3.25−3.43 (m, 10H, H_{5III}, H_{6IV}, and H_{1I}), 3.10−3.14 (m, 4H, H_{6II}), 2.70−2.95 (m, 8H, C_{5III}-S-CH_2-CH_2-NH), 2.36−2.47 (dt, 2H, ^1J = 12.1 Hz, ^2J = 4.0 Hz, H_{2Ieq}), 1.71−1.95 (p, 2H, J = 12.5 Hz, H_{2Iax}); ^{13}C NMR (125 MHz, D_2O) δ 174.8 (C═S), 107.9 (C_{1III}), 97.1 (C_{1IV}), 96.4 (C_{1II}), 77.7 (C_{3III}), 75.3 (C_{4III}), 73.9 (C_{4I}), 72.6 (C_{2III}), 72.4 (C_{6I}), 70.8 (C_{4II}), 70.4 (OCH_2CH_2, linker), 70.2 (OCH_2CH_2, linker), 69.8 (C_{5IV} or C_{3IV}), 69.6 (C_{5II}), 69.3 (C_{3II}), 68.3 (C_{5IV} or C_{3IV}), 68.1 (C_{4IV}), 67.8 (C_{5I}), 67.4 (C_{5III}-S-CH_2-CH_2-NH), 65.7 (C_{5III}-S-CH_2-CH_2-NH), 62.7 (C_{2II}), 58.5 (OCH_2CH_2NH, linker), 53.6 (C_{2IV}), 51.0 (C_{1I}), 50.9 (C_{3I}), 49.8, 40.8 (C_{5III}), 40.6 (C_{6IV}), 40.2 (C_{6II}), 28.4 (C_{2I}). MS MALDI-TOF calcd for $C_{58}H_{114}N_{16}O_{26}S_4$ ($M + H^+$), 1579.7, obsd: 1579.6. Anal. Calcd for $C_{58}H_{126}N_{16}O_{26}S_4Cl_{12}$: C, 34.53; H, 6.30; N, 11.11. Found: C, 34.12; H, 6.42; N, 10.93.

RESULTS AND DISCUSSION

Synthesis of 3. Modification of aminoglycoside-based conjugates have been primarily performed using two approaches. One approach uses the conjugation of aminoglycosides to various functionalities by linkage through the amines,[56] and a preferred second approach uses the primary hydroxyls present in the aminoglycosides,[43,57,58] such as the primary hydroxyl group (OH) on ring III of neomycin (Scheme 1). The latter derivatives provide a more suitable conjugation approach since the amino groups of aminoglycosides have been shown to participate in the ligand−DNA/RNA interaction.[59] The synthesis rests on the selective conversion of primary hydroxyl group (OH) on ring III of neomycin into a good leaving group (e.g., TPS, 2,4,6-triisopropylbenzenesulfonyl) as previously reported.[58] The displacement of the good leaving group (i.e., TPS) by 2-aminoethanethiol gave us neomycin amine **1**. The flexible linker, 2,2′-(ethylenedioxy)bis(ethylisothiocyanate) was then synthesized from the corresponding diamine with high yield (94%). The bis(isothiocyanate) linker **2** was coupled with neomycin amine **1** in the presence of DMAP catalyst, followed by deprotection with HCl/dioxane to yield the target conjugate **3** in good overall yields (~70% for two steps, Scheme 1) . The thiourea-based coupling approach to dimeric aminoglycosides complements the chemistries developed in the Tor, Wong, and Hergenbrother laboratories for screening of these conjugates against RNA targets.[30,52,55,60−63]

dx.doi.org/10.1021/ja108118v | J. Am. Chem. Soc. 2011, 133, 7361–7375

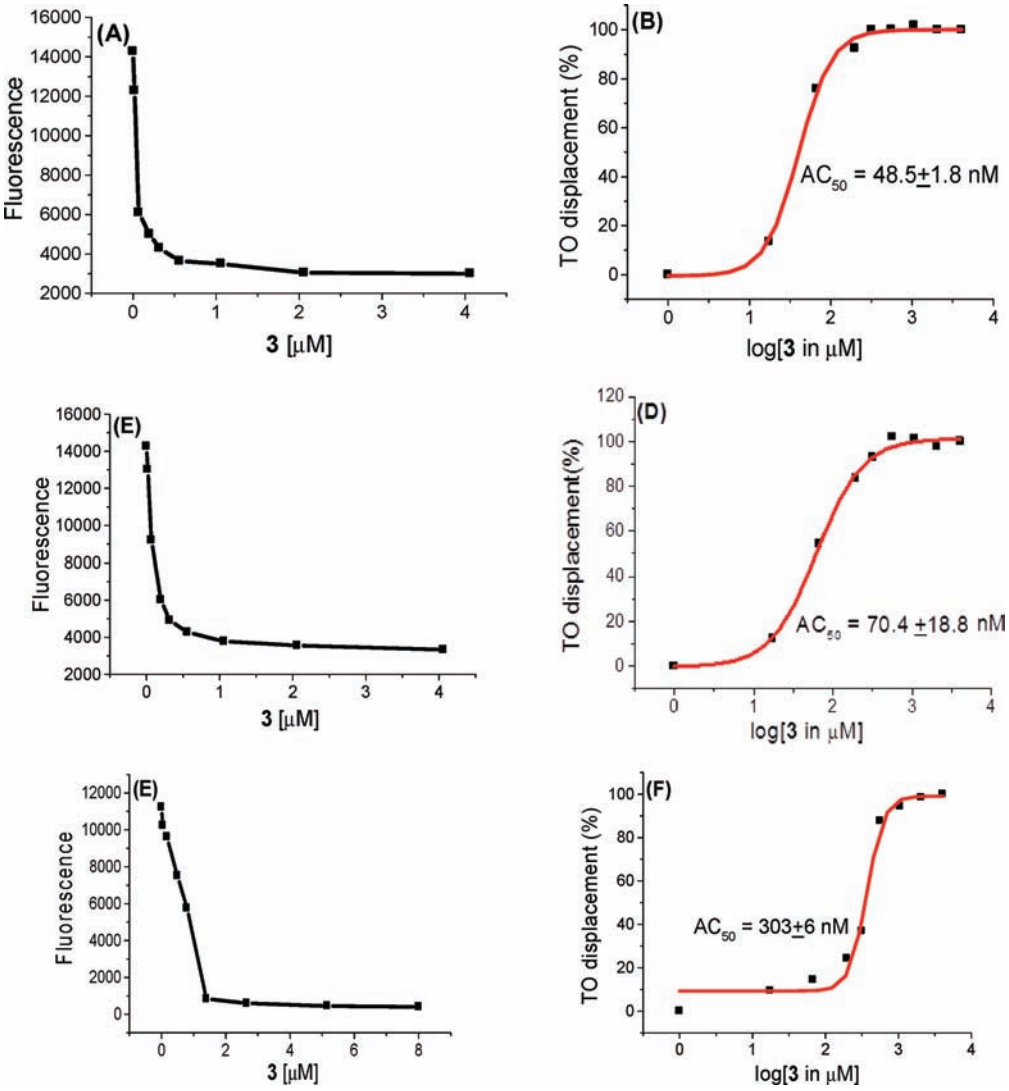

Figure 1. A graphical representation of the FID assay to calculate the AC_{50} value of **3** with various polynucleotides. (A) Plot showing decrease in the fluorescence intensity of *C. perfringens*−TO complex as a function of increasing concentration of **3**. (B) A sigmoidal fit between percentage of thiazole orange displaced from *C. perfringens* as a function of log [**3**]. (C) Plot showing decrease in the fluorescence intensity of *C. Thymus*−TO complex as a function of increasing concentration of **3**. (D) A sigmoidal fit between percentage of thiazole orange displaced from *C. Thymus* as a function log [**3**]. (E) Plot showing decrease in the fluorescence intensity of *M. lysodeiktius*−TO complex as a function of increasing concentration of **3**. (F) A sigmoidal fit between percentage of thiazole orange displaced from *M. lysodeiktius* as a function of log [**3**]. Buffer conditions: 100 mM KCl, 10 mM SC, 0.5 mM EDTA, pH 6.8. [polynucleotide] = 0.88 μM/bp, [TO] = 1.25 μM. The reported AC_{50} value in each case is an average of three separate experiments.

Ethidium Bromide Displacement Assay Shows the Preference of Dimer 3 toward AT-Rich DNA. To investigate the binding of **3** toward different DNA duplex sequences, we first monitored its binding to various DNA polynucleotides (*C. perfringens*, *C. Thymus*, and *M. lysodeiktius*) with varying GC and AT content. The FID assay was conducted by using ethidium bromide as an intercalator on a 96-well plate reader.[64]

Figure 1 depicts the typical 96-well plate assay between **3** and DNA polynucleotides, and the results are summarized in Table 1 with AC_{50} values (concentration of **3** required to displace 50% ethidium bromide from DNA). As shown in Table 1 and Figure 1, the AC_{50} values increase with increase in the GC base pair content of the DNA, suggesting the preference of **3** for AT-rich DNA duplexes.

Ethidium bromide FID assays were then carried out using homopolynucleotide DNA duplexes and a DNA triplex (see Supporting Information Figure S11). Table 2 summarizes the results and reveals some interesting facts. The AC_{50} value of **3** with poly(dA)·poly(dT) is lowest among polynucleotide duplexes, indicating that **3** shows the maximum affinity toward an AT-rich homopolynucleotide. Dimer **3** shows a higher selectivity for poly(dA)·poly(dT) when compared to the GC-rich polynucleotide, confirming previous results from Table 1. Additionally, **3** shows a significant preference for poly(dA)·poly(dT) duplex over the alternating $poly(dA\cdot dT)_2$ duplex. The AC_{50} values in Table 2 show that **3** binds much poorly to the DNA triplex when compared to the DNA duplex, in contrast to the results obtained with monomer neomycin, which has been shown by us to have a much higher affinity for the DNA triplex,[65] when compared a DNA duplex. The selectivity of **3** toward the DNA duplex is not limited to polynucleotide structures but is also seen with oligonucleotides (see Supporting Information Figure S12).

dx.doi.org/10.1021/ja108118v |*J. Am. Chem. Soc.* 2011, 133, 7361–7375

Table 1. FID-Based Determination of AC_{50} Values of 3 with Different Polynucleotides[a]

polynucleotide	GC content (%)	AC_{50} (nM)
C. perfringens	32	48.5 ± 1.8
calf thymus	42	70.4 ± 18.8
M. lysodeiktius	75	303.0 ± 6.0

[a] Buffer conditions: 100 mM KCl, 10 mM SC, 0.5 mM EDTA, pH 6.8. [DNA] = 0.88 μM/bp. [TO] = 1.25 μM. The reported AC_{50} value in each entry is an average of three separate experiments.

Table 2. FID-Based Determination of AC_{50} Values of 3 with Polynucleotides[a]

polynucleotide	AC_{50} values (nM)
poly(dG)·poly(dC)	140 ± 9
poly(dA)·poly(dT)	23 ± 2
poly(dA).2poly(dT)	990 ± 60
$poly(dA \cdot dT)_2$	61 ± 9

[a] The solutions were equilibrated for 1 h before taking the fluorescence scans. Buffer conditions: 100 mM KCl, 10 mM SC, 0.5 mM EDTA, pH 6.8. [polynucleotide] = 0.88 μM/strand. [TO] = 1.25 μM. The reported AC_{50} value in each entry is an average of three separate experiments.

The preference of **3** toward the DNA duplex vs DNA triplex will be discussed in more detail in a later section of UV thermal denaturation experiments. FID assays were then conducted using an oligonucleotide DNA hairpin duplex d[5′-A_{12}-x-T_{12}-3′] using the monomer and dimer ligand (neomycin and dimer **3**) (see Supporting Information Figure S13 and Table S1). Dimer **3** showed a ~100 fold lower AC_{50} than that of neomycin toward the intramolecular DNA hairpin duplex d[5′-A_{12}-x-T_{12}-3′] (see Supporting Information Table S1), suggesting that the AT duplex preference of the dimer over the monomer is not restricted to the polynucleotides but is also seen with deoxyoligonucleotides.

Determination of the Apparent DNA Binding Site Size of 3 Using CD and FID Titrations. CD spectroscopy was then used to determine the binding stoichiometry between dimer **3** and the host nucleic acids. The CD-derived binding site size is useful for the thermodynamic characterization of drug−DNA binding.[43,65] CD spectroscopy experiments were performed between three AT-rich DNA duplexes to determine the binding stoichiometry and to monitor the CD changes induced by DNA−ligand complexation. The CD spectrum of poly(dA)·poly(dT) exhibits two positive bands, 217 and 260 nm, and one negative band around 248 nm. The large positive band (217 nm) is equal in magnitude to the negative band (248 nm). Figure 2B depicts a group of CD spectra that result from the incremental addition of a concentrated solution of **3** to poly(dA)·poly(dT). The continuous addition of **3** results in changes in the CD spectrum which is indicative of the formation of a complex between the host DNA polynucleotide and **3** (Figure 2A). A close examination of CD spectra reveals the presence of an isoelliptic point, suggesting the formation of specific ligand−DNA complex. Figure 2B shows a plot between the change in the molar ellipticity vs r_{bd} (ratio of DNA base pairs/drug). The data were fit by linear least-squares fit, leading to an apparent stoichiometry of DNA binding to **3**. To further validate the stoichiometries obtained from CD titratons, FID titrations were also performed by using ethidium bromide as an intercalator.[64] The DNA duplexes were saturated with ethidium bromide solution, and incremental amounts of **3** were added continuously. The fluorescence scans were taken after each addition of **3** (Figure 2C). The additions of **3** were continued until there were no more changes observed in the fluorescence scans. The change in fluorescence was plotted versus r_{bd}, resulting in an inflection point (Figure 2D) which represents another independent estimate of the binding stoichiometry of complex formed between DNA and **3**.

DNA−**3** stoichiometries obtained from CD spectroscopies and fluorescence titrations were quite comparable and show a binding size of 10−12 base pair for **3** binding to AT-rich DNA duplexes. Similar studies were performed with $poly(dA \cdot dT)_2$ (see Supporting Information Figure S14), d[5′-$A_{30}T_{30}$-3′] (see Supporting Information Figure S15), and the poly(dG)·poly(dC) DNA duplex to determine the apparent binding site size of dimer **3**. The results from the fluorescence titrations are summarized in Table 3. The binding site size of **3** with all of the nucleic acids varies between 9 and 12 base pairs/ligand.

Nanomolar Binding of 3 to a Model Deoxyoligonucleotide Duplex: FID and Salt Dependence of Binding. The results of the FID and CD titrations suggest that the ideal AT-rich DNA binding site size for **3** lies between 10 and 12 base pairs/ligand (Table 3). On the basis of these results, we designed and prepared a 12-mer AT-rich DNA hairpin duplex d[5′-A_{12}-x-T_{12}-3′] as well as other DNA duplexes with various lengths and base contents to study their binding with **3**. FID (see Supporting Information Figures S16 and S17) and CD (see Supporting Information Figure S18) titrations between the hairpin duplex d[5′-A_{12}-x-T_{12}-3′] and **3** result in a binding stoichiometry of 1:1, as expected from a binding site size of ~12 base pairs/ligand. FID titration was performed between **3** and d[5′-A_{12}-x-T_{12}-3′], and Scatchard analysis was conducted to yield a high binding constant (Figure 3, $K_a = 2.26 \times 10^8$ M^{-1} at 50 mM KCl).[64]

Salt-dependent binding studies were carried out to assess the electrostatic contribution of binding between **3** and d[5′-A_{12}-x-T_{12}-3′] at 50, 100, and 150 mM KCl (Figure 3, and Figures S16 and S17). The results are summarized in Table 4. A plot of log (K_a) as a function of log[K^+] shows that the binding constant decreases with increasing salt concentration (Figure 4) and suggests the formation of about three ion pairs[66] between **3** and DNA. Further pH- and salt-dependent studies are ongoing for the complete thermodynamic characterization of **3** with AT-rich DNA duplexes.

Dimer 3, Contrary to Neomycin, Significantly Increases the T_m of AT-Rich DNA Duplexes. We have previously reported the effect of antibiotics, specifically neomycin, on the thermal stability of DNA−RNA hybrids and triple helices.[29,65] Herein, we report the interaction of **3** with AT-rich DNA duplexes using UV spectroscopy.

UV thermal denaturation experiments were performed between poly(dA)·2poly(dT) and ligands neomycin and **3**. In the absence of ligand, the UV thermal denaturation profile of poly(dA)·2poly(dT) shows two transitions (Figure 5A and 5B, denoted as "control") and the dissociation of triplex into duplex (at 34 °C) followed by the dissociation of duplex into single strands (at 72.5 °C). The UV thermal denaturation profile was monitored at 284 nm where the triplex melting transition is more prominent in comparison to 260 nm. A UV thermal denaturation experiment shows that neomycin stabilizes poly(dA)·2poly(dT) by ~7 °C and has no effect on the stability of poly(dA)·poly(dT) (Figure 5 B) at r_{bd} = 3, an observation consistent with our

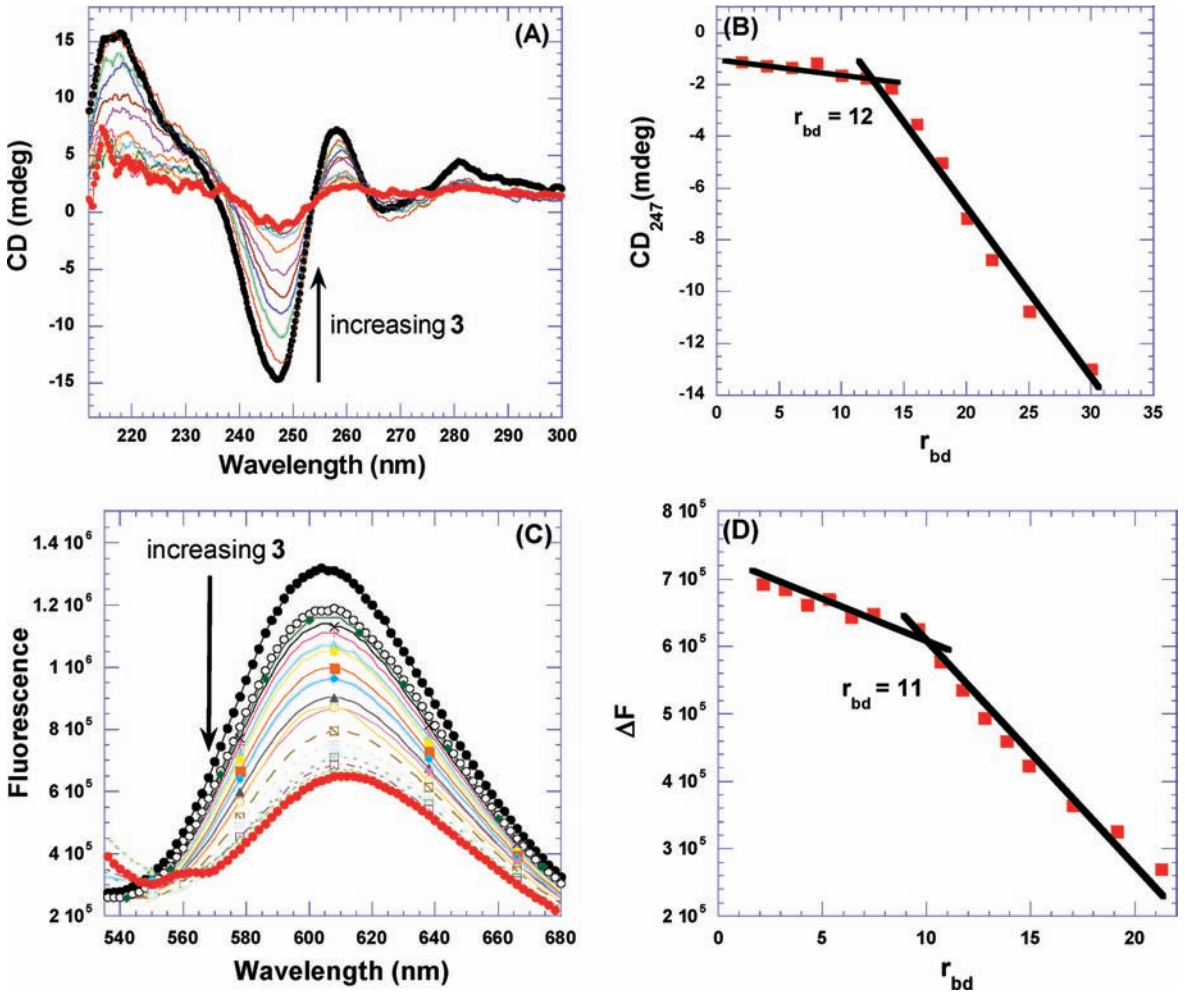

Figure 2. (A) CD titration of poly(dA)·poly(dT) with increasing concentration of **3**. The figure represents normalized molar ellipticity for CD titration of poly(dA)·poly(dT) with **3**. The continuous changes in the CD spectra correspond to the incremental amount of **3** ranging from an r_{bd} of 0 to 30. (B) A plot of normalized molar ellipticity versus r_{db} for CD titration of poly(dA)·poly(dT) with **3**. The continuous lines in the plot reflect the linear least-squares fits of each apparent linear domain of the experimental data (filled circles) before and after the apparent inflection point. Molar ellipticity is per molar base pair, and r_{bd} = ratio of the base pair/drug. (C) Raw fluorescence emission spectrum of poly(dA)·poly(dT)−EtBr complex with increasing concentration of **3**. A decrease in fluorescence intensity (at 618 nm) of the poly(dA)·poly(dT)−EtBr complex with increasing concentration of **3** is observed. (D) The plot of change in the fluorescence as a function of r_{bd} gives the binding site size of **3** with poly(dA)·poly(dT). The solution was incubated for 1 h at 20 °C before titrating with **3**. The solutions were equilibrated for 5 min after each ligand addition, and before taking the fluorescence emission scans. Buffer conditions: 100 mM KCl, 10 mM SC, 0.5 mM EDTA, pH 6.8. [DNA] = 10 μM/bp (for fluorescence titration) and 40 μM/bp (for CD titration).

previous results.[65] On the contrary, **3** stabilizes poly(dA)·poly(dT) by ~12 °C at a much lower ligand concentration and the triplex denaturation disappears (r_{bd} = 12, Figure 5 A), suggesting the destabilization of DNA triplex in the presence of **3**.

A UV thermal denaturation experiment was performed between DNA triplex with a gradual increase in the concentration of **3** (0 to 1.25 μM, r_{bd} up to 12 base pairs/drug). The thermal denaturation temperature of duplex ($\Delta T_{m2\rightarrow1}$) increases while the transition for triplex ($\Delta T_{m3\rightarrow2}$) gradually disappears with an increase in the concentration of **3**. During the formation of DNA triplex from the corresponding duplex and single strand, the third strand, poly(dT), binds into the major groove via Hoogsteen base pairing and divides the Watson−Crick major groove into two asymmetric parts: the minor part of the major groove (Crick−Hoogsteen (C−H) groove) and the major part of the major groove (Watson−Hoogsteen (W−H)). Neomycin fits well into the major groove of the DNA triplex (Watson−Hoogsteen (W−H)) with a good shape and potential complementarity that is observed in its ability to stabilize the DNA triplex.[29,65] However, neomycin does not have a suitable binding

Table 3. Binding Site Sizes Calculated by FID Titrations between 3 and Various Nucleic Acids[a]

nucleic acid	binding site size (bp)
poly(dA)·poly(dT)	11
poly(dA·dT)$_2$	10
poly(dG)·poly(dC)	9
d[5′-$A_{30}T_{30}$-3′]	10

[a] Buffer conditions: 100 mM KCl, 10 mM SC, 0.5 mM EDTA, pH 6.8. T = 20 °C. [polynucleotides] = 10 μM/bp. [EtBr] = 5 μM. d[5′-$A_{30}T_{30}$-3′] = 0.50 μM/duplex, [TO] = 15 μM.

dx.doi.org/10.1021/ja108118v |*J. Am. Chem. Soc.* 2011, 133, 7361–7375

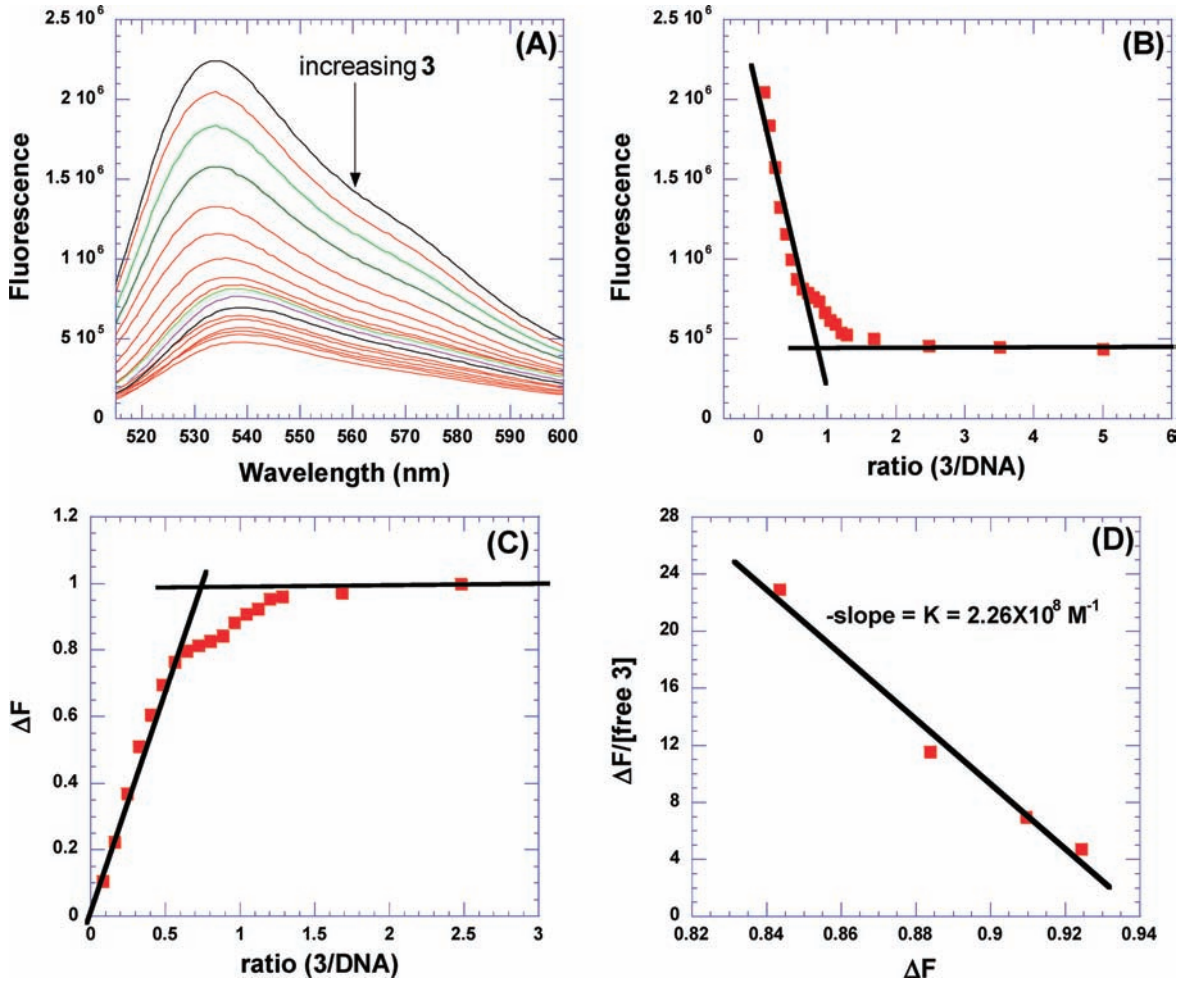

Figure 3. FID titration of **3** with intramolecular duplex d[5′-A_{12}-x-T_{12}-3′]. (A) Raw fluorescence emission spectrum in the presence of increasing concentrations of **3**. (B) A decrease in fluorescence intensity (at 532 nm) of the DNA—TO complex with increasing concentrations of **3** results in a saturating binding plot. (C) Plot between change in fluorescence intensity and concentration of **3**. (D) Scatchard analysis for determination of K_a between **3** and duplex d[5′-A_{12}-x-T_{12}-3′]. The solution was incubated for 1 h at 15 °C before titrating it with **3**. The solutions were equilibrated for 5 min after each ligand addition, and before taking the fluorescence emission scans. Buffer conditions: 50 mM KCl, 10 mM SC, 0.5 mM EDTA, pH 6.8. d[5′-A_{12}-x-T_{12}-3′] = 1 μM/strand, [TO] = 6 μM. T = 20 °C.

pocket in the wider groove of B- and B*-form DNA duplex and is thus not expected to lead to thermal stabilization of the neomycin—DNA duplex complex. Dimer **3** was designed from two monomeric neomycin units connected through a flexible linker so that the dimer will present a higher potential and shape complementarity to the DNA duplex major groove, when compared to neomycin. The major groove of DNA duplex is the likely binding site of **3** and is substantiated by the following observations: (a) **3** thermally stabilizes the DNA duplex and destabilizes the DNA triplex (Figure 6), suggesting that **3** competes with the dT triplex-forming strand that binds in the major groove of duplex DNA; (b) the larger binding size of the dimer (10—12 base pairs), which would be expected of a ligand traversing the wide B-form DNA major groove; (c) when the FID studies were conducted using poly(dA)·2poly(dT) triplex and poly(dA)·poly(dT) duplex (Table 2), a much higher AC_{50} for binding to the triplex over duplex was observed, suggesting that as opposed to neomycin, the dimer **3** clearly favors the duplex. The latter observation is also consistent with the hypothesis that **3** competes with the dT triplex-forming strand that binds in the major groove of duplex DNA.

Table 4. Binding Affinity of 3 with Intramolecular Duplex d[5′-A_{12}-x-T_{12}-3′] at Different Salt Concentrations[a]

salt concentration (KCl in mM)	binding constant ($\times 10^6$), M^{-1}
50	226.0
100	117.0
150	7.6

[a] Buffer conditions: 10 mM SC, 0.5 mM EDTA, pH 6.8. d[5′-A_{12}-x-T_{12}-3′] = 1 μM/strand. [TO] = 6 μM. T = 20 °C.

Similar results of DNA duplex stabilization were obtained with poly(dA·dT)$_2$ in the presence of neomycin and **3** (Supporting Information Figures S19 and S20). **3** thermally stabilizes poly(dA·dT)$_2$ (r_{bd} = 10) with a $\Delta T_m \sim 11$ °C while neomycin has no effect on the thermal stability of poly(dA·dT)$_2$. The thermal stabilization of AT-rich duplexes by **3** was not limited to polynucleotides but also observed with oligonucleotides (as shown in Tables 5 and 6; see Supporting Information Figures S21 and S22). Further UV thermal denaturation experiments were carried out between DNA oligonucleotides with varying base composition

dx.doi.org/10.1021/ja108118v |J. Am. Chem. Soc. 2011, 133, 7361–7375

in the presence of **3**, and the results are summarized in Tables 5 and 6.

After inspection of the UV thermal denaturation data, the following observations were made: (1) Consistent with the results from the binding of **3** to polynucleotides, all AT-rich deoxyoligonucleotides show thermal stabilization in the presence of **3** (Table 5). (2) The UV thermal stability of deoxyoligonucleotides increases with an increase in the concentration of **3** (Figure 7 and Table 6; see Supporting Information Figure S22). (3) The thermal stability of DNA duplexes in the presence of **3** increases with increase in the length of DNA duplexes. The thermal stability of DNA duplexes in the presence of **3** under saturating ligand concentrations follows the order for AT-rich duplexes, d[5′-A_8T_8-3′] < d[5′-$A_{30}T_{30}$-3′] < poly(dA)·poly(dT). (4) T_m studies with **3** and DNA duplexes with high GC content (see Supporting Information Figure S21) lead to multiphasic denaturation profiles, suggesting a more complex binding phenomenon. (5) Neomycin shows no effect on the thermal stabilization of AT-rich deoxyoligonucelotides or polynucleotides.

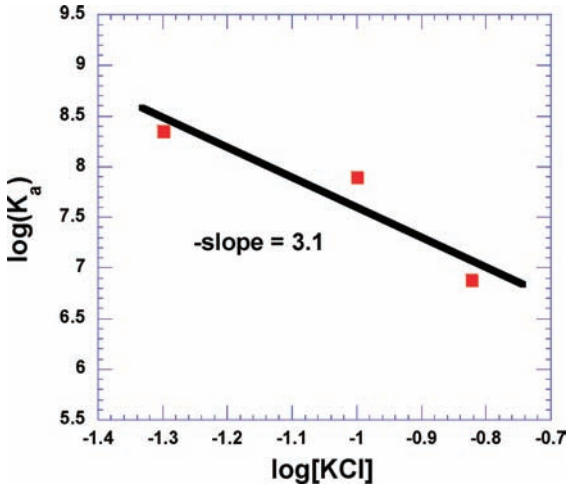

Figure 4. Plot showing the salt dependence of binding between **3** and d[5′-A_{12}-x-T_{12}-3′] in 10 mM SC, 0.5 mM EDTA, pH 6.8. The experimental data were fit with linear regression, and the solid black line reflects the linear fit. T = 20 °C.

ITC-Derived Thermodynamics of Binding of 3 to Deoxyoligonucleotides. ITC titrations were performed to characterize the binding of **3** with DNA duplexes with varying base compositions, lengths, and conformations. The corrected ITC titrations are shown in Figures 8 and 9 (also see Supporting Information Figures S23 and S24), and the ITC-derived thermodynamic parameters are summarized in Tables 7 and 8. Each peak in the upper panel (Figure 8) in every titration is the heat generated by the single injection of **3** to the corresponding DNA duplex solution. The area under each heat burst curve was determined by integration to obtain the heat associated with each injection. The corrected heat for ligand−DNA complexation was calculated by subtracting the heat of dilution of **3** obtained using the ITC titration of **3** in buffer. The following trends are noticeable from the thermodynamic parameters summarized in Tables 7 and 8. (1) There are two binding events observed during the complexation of **3** with most AT-rich DNA duplexes which were fitted using a two independent site binding model (Origin 5.0). (2) The first binding site is the high affinity site with a binding constant ~ 10^8 M^{-1}, almost 50−100 fold higher than the binding constant of second binding event (Tables 7 and 8). (3) The stoichiometry for the first binding site is ~1 between **3** and the DNA duplex for continuous AT-rich duplexes (and 12−14 base pairs for d[5′-A_{30}·T_{30}-3′]), corroborating the results obtained from CD and fluorescence titrations. The stoichiometry for the second binding site is ~3−4 (drug/DNA duplex) for most deoxyoligonucleotides, reflecting a nonspecific binding likely resulting from the electrostatic interactions between **3** and the DNA duplex. (4) The binding affinity of **3** toward the DNA duplexes has the following order: continuous AT-rich sequence, d[5′-$G_3A_5T_5C_3$-3′] (D3) > alternate AT-rich sequence, d[5′-$G_3(AT)_5C_3$-3′] (D9) > GC-rich sequences,>d[5′-$G_3G_5C_5C_3$-3′] (D1) ~d[5′-$A_3G_5C_5T_3$-3′] (D4) (Figures 8 and 9 and Table 7). (5) The thermodynamic signatures for the first binding event are significantly different from the second binding event. For continuous AT-rich sequences, the first binding event is predominantly entropy driven, while on the other hand, the second binding event is enthalpy driven. For the remainder of the duplexes (alternate AT-rich duplex or the GC-rich duplex), the first binding

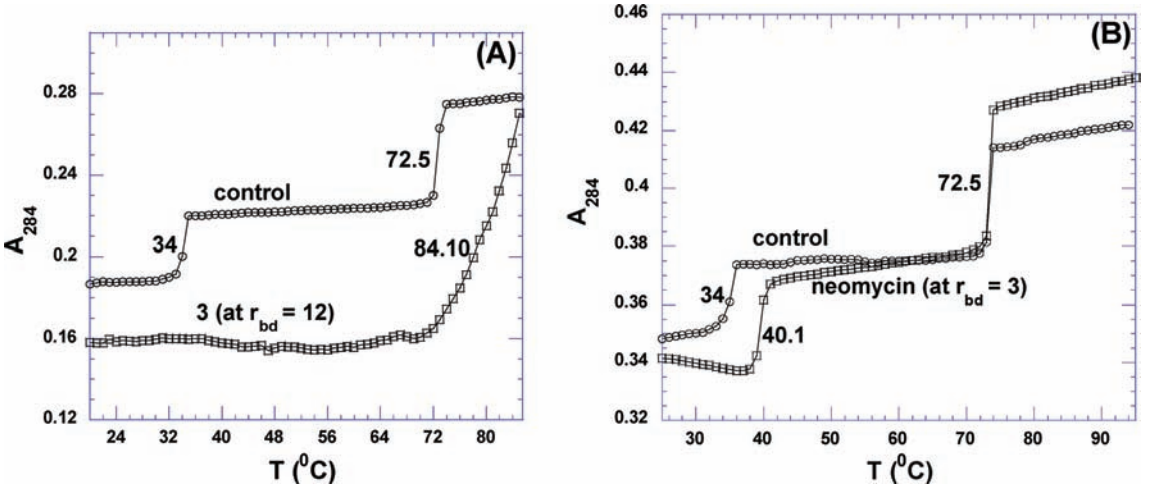

Figure 5. UV thermal denaturation profile of poly(dA)·2poly(dT) with ligands. (A) UV thermal denaturation profile of poly(dA)·2poly(dT) in the absence (circle) and presence (square) of **3** (at r_{bd} = 12). (B) UV thermal denaturation profile of poly(dA)·2poly(dT) in the absence (circle) and presence (square) of neomycin (at r_{bd} = 3). Buffer conditions: 100 mM KCl, 10 mM SC, 0.5 mM EDTA, pH 6.8. [DNA] = 15 μM/triplex.

dx.doi.org/10.1021/ja108118v |*J. Am. Chem. Soc.* 2011, 133, 7361–7375

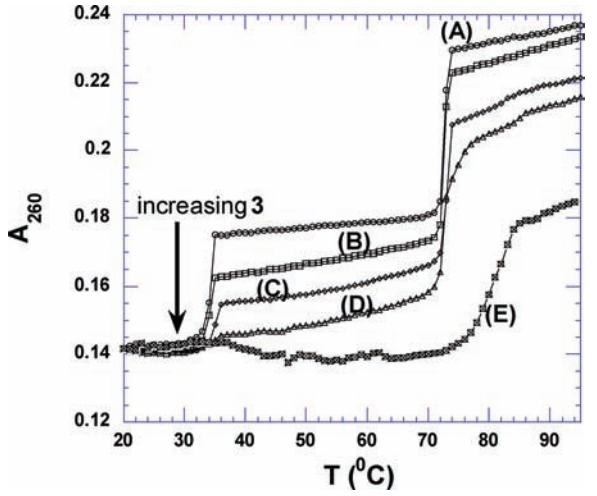

Figure 6. UV thermal denaturation profile of poly(dA)·2poly(dT) in the presence of **3** at (A) 0 μM, (B) 0.25 μM (r_{bd} = 60), (C) 0.50 μM (r_{bd} = 30), (D) 1.0 μM (r_{bd} = 15), and (E) 1.25 μM (r_{bd} = 12). Buffer conditions: 150 mM KCl, 10 mM SC, 0.5 mM EDTA, pH 6.8. [DNA] = 15 μM/bt.

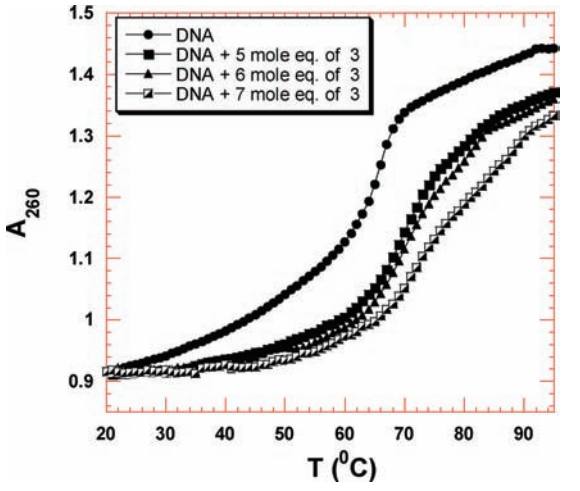

Figure 7. UV thermal denaturation profile of d[5′-$A_{30}T_{30}$-3′] in the presence of **3** at 5 μM (5 mol equiv), 6 μM (6 mol equiv), and 7 μM (7 mol equiv). Buffer conditions: 100 mM KCl, 10 mM SC, 0.5 mM EDTA, pH 6.8. d[5′-$A_{30}T_{30}$-3′] = 1 μM/duplex.

Table 5. Change in $T_{m2\rightarrow1}$ (at r_{dd} = 1.0, where r_{dd} = ratio of the duplex/drug) in the Presence of 3[a]

oligonucleotide	ΔT_m (°C)
d[5′-A_8T_8-3′]	6.5
d[5′-GA_7T_7C-3′]	5.5
d[5′-$G_2A_6T_6C_2$-3′]	4.9
d[5′-$G_3A_5T_5C_3$-3′]	5.0

[a] Buffer conditions: 100 mM KCl, 10 mM SC, 0.5 mM EDTA, pH 6.8. The melting rate was 0.2 °C/min. [DNA] = 1 μM/duplex.

Table 6. Change in $T_{m2\rightarrow1}$ (at r_{dd} = 5.0, 6.0, and 7.0) for Denaturation of d[5′-$A_{30}T_{30}$-3′] in the Presence of 3[a]

concn of **3** (μM)	T_m (°C)	ΔT_m (°C)
0	64.9	0.0
5	72.7	7.8
6	74.1	9.2
7	77.9	13.0

[a] Buffer conditions: 100 mM KCl, 10 mM SC, 0.5 mM EDTA, pH 6.8. The melting rate was 0.2 °C/min. [DNA] = 1 μM/duplex.

event is either enthalpy driven (duplex D1) or shows a much lesser contribution to the free energy of binding from the entropy (D9). When we compare the thermodynamics of binding of deoxyoligonucleotides D3 to D9, the enthalpic contributions to the binding are almost equivalent (−2.48 versus −2.73 kcal/mol), but D3 shows a much larger contribution to free energy of binding from entropy ($T\Delta S_1$ = 8.96 versus 4.82 kcal/mol), leading to a 50 fold higher affinity of dimer **3** with D3 than with D9. Additionally, while there are large variations in K_1 values for the first binding event, the K_2 values for all the deoxyoligonucleotides remain relatively constant (D2, D3, D7, D8, Table 8), suggesting a nonspecific binding event. (6) The alternating AT duplex D9 shows the weakest affinity among the AT-rich DNA duplexes. The DNA oligonucleotide D3 has a 10 base pair AT tract with one A to T switch, whereas the oligonucleotide D9 contains a 10 base pair stretch of alternating AT base pairs (9 switches). The ITC-derived binding constant of **3** with D3 is significantly higher (50 fold) than with D9. Attempts were made to make a similar comparison with a longer sequence set, 22-mer oligonucleotide D7 and its AT-rich alternate version (sequence D10). However, the ITC profile of sequence D10 under similar solution conditions exhibited multiple binding events that could not be fit to derive useful thermodynamic data (see Supporting Information Figure S24E,F). (7) The binding of **3** with DNA is clearly base content dependent. In general, dimer **3** binds more tightly to AT-rich DNA (D2, D3, D5, and D6) than to GC-rich DNA such as D1 and D4 (Table 7). Additional evidence for this conclusion comes from the comparison of the binding of **3** with two 22-mer DNA duplexes, D7 and D8, that contain polypurine and polypyrimidine single strands. The former contains 12 consecutive AT base pairs, and the latter has 12 mixed base pairs in the same region. ITC profiles indicate that the binding constant of D7 with **3** is $(8 \pm 3) \times 10^7$ M^{-1}, which is 4.5 fold higher than that of D8 with **3**. The binding constants have no noticeable difference in the second binding event. Duplexes D7 and D8 both adopt a canonical B-form conformation, as they do not contain continuous A tracts or G tracts, as also confirmed by CD spectroscopy. (8) Inclusion of continuous GC base pairs in the middle of the sequence (D3 versus D1 and D4), which can lead to an A-form DNA conformation, significantly alters the ITC profiles such that there is a single low affinity binding site where multiple drugs bind. The duplex affinities of **3** with D1 and D4 are lowered by a factor of 100−1000, when compared to the affinity of **3** with D3.

DNA Duplex Binding of Monomer versus Dimer. ITC Studies of Neomycin and 3 Binding to A- and B-Form DNA Duplexes. The binding affinities of ligands **3** and neomycin were then compared for AT- and GC-rich duplexes. ITC titrations were performed between d[5′-$A_3G_5C_5T_3$-3′] and ligands **3** and neomycin under similar conditions, and the thermodynamic parameters are summarized in Table 9. Dimer **3** shows only ~3 fold higher binding affinity than neomycin toward the GC-rich DNA duplex D4. The shape of the ITC titration reveals that there is one binding event taking place with both ligands, but **3** shows a binding stoichiometry of ~3:1, whereas neomycin binds

dx.doi.org/10.1021/ja108118v |J. Am. Chem. Soc. 2011, 133, 7361–7375

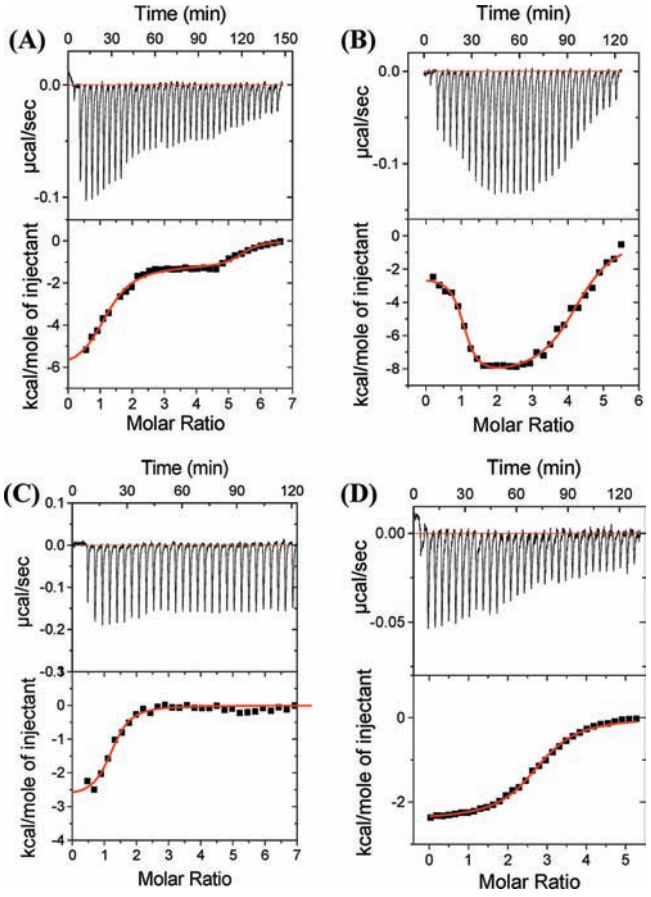

Figure 8. ITC profile of **3** with (A) d[5′-A_{12}-x-T_{12}-3′], (B) d[5′-$G_3A_5T_5C_3$-3′], (C) d[5′-$G_3(AT)_5C_3$-3′], and (D) d[5′- $A_3G_5C_5T_3$-3′]. Top panel: ITC titrations represent the heat burst curves, and each heat burst curve is a result of a 9 μL injection of 125 μM **3** into the DNA duplex. The area under each heat burst curve was calculated by integration and yields the associated injection heats which were then plotted as a function of the molar ratio of drug to DNA in the lower panel in each figure. Lower panel: Corrected injection heats plotted as a function of the [drug]/DNA ratio. Buffer conditions: 100 mM KCl, 10 mM SC, 0.5 mM EDTA, pH 6.8. T = 25 °C. [DNA] = 4 μM/duplex. [**3**] = 125 μM.

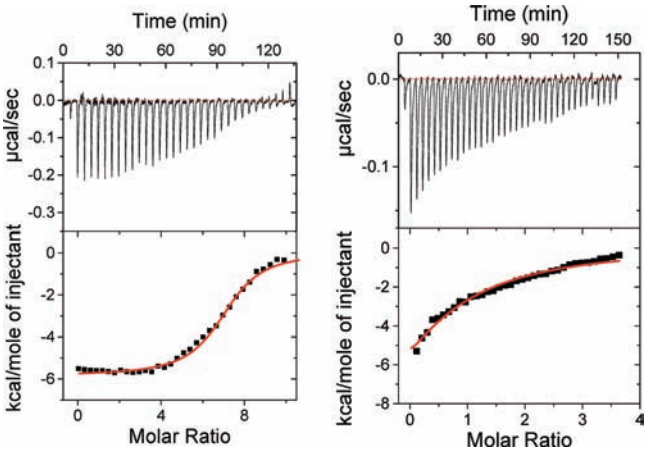

Figure 9. ITC titration profile of d[5′-$G_3G_5C_5C_3$-3′] with **3** (left) and d[5′-$A_3G_5C_5T_3$-3′] with neomycin (right). Top panel: ITC titrations represent the heat burst curves, and each heat burst curve is a result of a 9 μL injection of ligands into the duplex DNA. The area under each heat burst curve was calculated by integration and yields the associated injection heats, which were then plotted as a function of molar ratio of drug to DNA in the lower panel in each figure. Lower panel: Corrected injection heats plotted as a function of the [drug]/DNA ratio. Buffer conditions: 100 mM KCl, 10 mM SC, 0.5 mM EDTA, pH 6.8. T = 25 °C. [**3**] = 225 μM. [DNA] = 6 μM/duplex, [neomycin] = 250 μM.

with a stoichiometry of 1:1 (Figure 9). The lower binding constant and a higher stoichiometry of **3**:D4 complexation (as compared to AT-rich duplexes) suggests that **3** binds to the GC-rich duplex D4 (as well as D1) through nonspecific electrostatic interactions. Our finding that **3** has higher binding affinity toward D3 than D1 and D4 can be rationalized on the basis of conformation of the DNA duplexes used in the study. The CD spectrum of DNA duplex d[5′-$A_3G_5C_5T_3$-3′] and d[5′-$G_3A_5T_5C_3$-3′] are shown under the same solution conditions (Figure 10). The CD spectrum of DNA duplex d[5′-$G_3A_5T_5C_3$-3′] exhibits a positive band at 280 nm and a negative band around 248 nm with almost equal intensities, representative of a B-form DNA conformation.[67] On the other hand, the CD spectrum of DNA duplex d[5′-$A_3G_5C_5T_3$-3′] exhibits a positive band at 262 nm and a negative band around 240 nm, which represents an A-form DNA conformation.[67,68] Sequence D1 shows an A-form CD spectrum identical to sequence D4, and ITC shows almost seven molecules of **3** binding to the duplex (Figure 9), suggesting a nonspecific complexation process. Neomycin binding to D1 resembles the binding of neomycin to D4, with a slightly higher affinity being observed for D1 than for D4 (Table 9). The A-form DNA conformation represents a structure with a narrower and deeper major groove and a wider and shallower minor groove, whereas the major groove of B and B*-form DNA is much wider. A combination of ITC and CD data analysis suggests that **3** shows a higher binding affinity toward B-form DNA when compared to A-form DNA. Again, the major groove remains a likely binding site, since the higher affinity of the larger ligand **3** is observed with DNA conformations with a wider major groove (B, B*) whereas the smaller monomer ligand neomycin prefers to bind the DNA conformations with narrower major grooves (A-form).

Similar studies were conducted between ligands **3** and neomycin and duplex d[5′-$G_3A_5T_5C_3$-3′]. Under identical solution conditions, we were not able to determine the binding constant between d[5′-$G_3A_5T_5C_3$-3′] and neomycin because of the extremely weak signal in ITC titration (see Supporting Information Figure S25). Neomycin shows very weak binding affinity toward AT-rich DNA duplexes. On the basis of previous results of neomycin binding toward the AT-rich DNA duplex ($K_a < 10^5$ M^{-1}) and triplex, we estimate that **3** has at least a 1000 fold higher affinity than neomycin for the B*-form AT-rich DNA duplexes.[65]

Thiazole Orange FID Assay for 512-Member Deoxyoligonucleotide Hairpin Library with 3. The thiazole orange displacement assay was performed between **3** and 512 hairpin duplexes that varied in their A and T content and placements. The FID assay is one of the simpler assays used for determining the sequence selectivity of ligands.[64,69] Boger and co-workers[64] have developed this assay for DNA duplexes, and the assay has been later utilized for studying ligand binding to DNA triplexes[70] and DNA quadruplexes.[71] From our previous experiments (ITC, CD, and fluorescence titrations), we have determined the DNA binding site size of **3** (~10−12 base pairs). Data presented from

dx.doi.org/10.1021/ja108118v |*J. Am. Chem. Soc.* 2011, 133, 7361–7375

Table 7. ITC-Derived Thermodynamic Profiles for the Binding of 3 with Different Oligonucleotides[a]

DNA sequence no.	DNA sequence	N_1	K_1 (M^{-1}) × 10^7	ΔH_1(kcal/mol)	$T\Delta S_1$ (kcal/mol·K)
D1	d[5′-$G_3G_5C_5C_3$-3′]	7.04 ± 0.04	0.27 ± 0.02	−5.83 ± 0.04	2.95
D2	d[5′-$G_2A_6T_6C_2$-3′]	0.82 ± 0.02	12.9 ± 3.4	−5.16 ± 0.03	5.90
D3	d[5′-$G_3A_5T_5C_3$-3′]	1.01 ± 0.02	25.3 ± 10.0	−2.48 ± 0.02	8.96
D4	d[5′-$A_3G_5C_5T_3$-3′]	2.64 ± 0.09	0.077 ± 0.001	−3.19 ± 0.01	4.82
D5	d[5′-A_{12}-x-T_{12}-3′]	1.16 ± 0.06	28.2 ± 12.0	−6.34 ± 0.46	5.18
D6	d[5′-$A_{30}T_{30}$-3′]	4.30 ± 0.16	129.2 ± 54.1	−7.49 ± 0.16	5.06
D7[b]	d[5′-$A_2G_3A_{12}G_3A_2$-3′]	1.95 ± 0.10	8 ± 3	−2.1 ± 1.8	7.5
D8[b]	d[5′-A_2GAG_2AGAG $A_2GAGAG_2AGA_2$-3′]	2.4 ± 0.8	1.78 ± 1.00	−0.85 ± 0.6	9.74
D9	d[5′-$G_3(AT)_5C_3$-3′]	1.19 ± 0.05	0.54 ± 0.15	−2.73 ± 0.16	6.25
D10[b]	d[5′-$A_2G_3(AT)_6G_3A_2$3′]	NA	NA	NA	NA
D11	d[5′-$(AT)_8$-3′]	0.97 ± 0.04	5.88 ± 2.90	−9.13 ± 0.51	1.46

[a] Buffer conditions: 100 mM KCl, 10 mM SC, 0.5 mM EDTA, pH 6.8 at 25 °C. [DNA] = 4 μM/duplex, [**3**] = 125 μM. [b] [DNA] = 4 μM/duplex, [**3**] = 440 μM.

Table 8. ITC-Derived Thermodynamic Profiles for the Binding of 3 with Different Oligonucleotides[a]

DNA sequence no.	DNA sequence	N_2	K_2(M^{-1}) X10^6	ΔH_2(kcal/mol)	$T\Delta S_2$ (kcal/mol.K)
D1	d[5′-$G_3G_5C_5C_3$-3′]	NA	NA	NA	NA
D2	d[5′-$G_2A_6T_6C_2$-3′]	3.19 ± 0.03	2.15 ± 0.13	−12.09 ± 0.09	−2.95
D3	d[5′-$G_3A_5T_5C_3$-3′]	3.25 ± 0.05	2.69 ± 0.39	−8.65 ± 0.02	0.12
D4	d[5′-$A_3G_5C_5T_3$-3′]	NA	NA	NA	NA
D5	d[5′-A_{12}-x-T_{12}-3′]	4.19 ± 0.11	12.2 ± 5.7	−1.17 ± 0.08	8.40
D6	d[5′-$A_{30}T_{30}$-3′]	2.01 ± 0.17	71.1 ± 14.0	−11.44 ± 0.54	0.53
D7[b]	d[5′-$A_2G_3A_{12}G_3A_2$-3′]	7.0 ± 0.1	3.80 ± 0.06		
D8[b]	d[5′-A_2GAG_2AGAG $A_2GAGAG_2AGA_2$-3′]	9.4 ± 0.8	3.3 ± 1.0		
D9	d[5′-$G_3(AT)_5C_3$-3′]	NA	NA	NA	NA
D10[b]	d[5′-$A_2G_3(AT)_6G_3A_2$-3′]	NA	NA	NA	NA

[a] Buffer conditions: 100 mM KCl, 10 mM SC, 0.5 mM EDTA, pH 6.8 at 25 °C. [DNA] = 4 μM/duplex, [**3**] = 125 μM. [b] [DNA] = 4 μM/duplex, [**3**] = 440 μM.

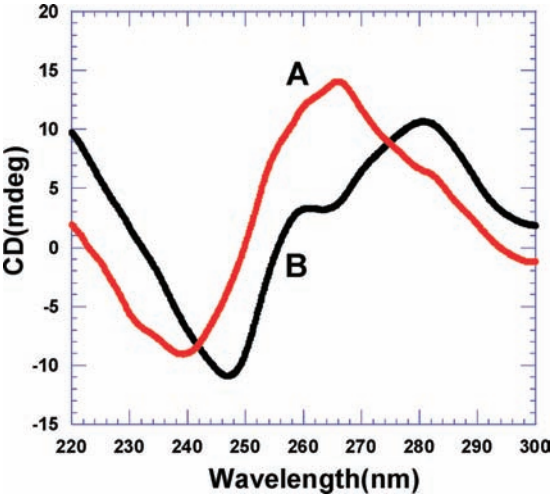

Figure 10. CD spectra of the DNA sequences (A) d[5′-$A_3G_5C_5T_3$-3′] and (B) d[5′-$G_3A_5T_5C_3$-3′]. Buffer conditions: 100 mM KCl, 10 mM SC, 0.5 mM EDTA, pH 6.8 at 25 °C. [DNA] = 4 μM/duplex.

our studies have shown that **3** prefers to bind to continuous AT-rich sequences over alternating AT sequences. To further investigate the preference of **3** for nonalternating versus alternating AT sequences, we have designed a 12-mer DNA duplex hairpin library (512 hairpins; see Supporting Information Table S2) that contains one GC base pair on each end and the ten AT base pairs in the middle of the sequence have been varied. Thiazole orange was utilized as an intercalator for the assay, and the assay was performed at 1:1 drug/DNA ratio in duplicate, with the error values at ±10%. Results show a DNA sequence preference for **3** that is similar to what we observed with FID and ITC titrations and are discussed below.

Binding of **3** was examined against a library of 512 DNA hairpin oligonucleotides, and the results are depicted in Figure 11. Data in Figure 11 show the percent fluorescence for all the 512 hairpin sequences in the presence of dimer **3** (Figure 11A); the insets show the sequences of the hairpins that show the highest percent fluorescence (Figure 11D, weakest binders) and lowest percent fluorescence (Figure 11C, strongest binders). When dimer **3** binds a hairpin with high affinity, a significant amount of TO is displaced, lowering the % fluorescence. Figure 11 shows that **3** exhibits a clear selectivity toward continuous AT-rich sequences, as the 20 highest affinity hairpins (as identified by high TO displacement = lowest % fluorescence) contain very few A to T switches. On the other hand, the 20 lowest affinity hairpins (as identified by low TO displacement = highest % fluorescence) show a large number of A to T switches with one of the lowest affinity hairpin being the sequence with the maximum possible

dx.doi.org/10.1021/ja108118v |J. Am. Chem. Soc. 2011, 133, 7361–7375

Table 9. Comparison of ITC-Derived Thermodynamic Profiles of 3 and Neomycin with A form duplexes[a]

ligand:DNA	N_1	K_1 (M^{-1}) × 10^5	ΔH_1 (kcal/mol)	$T\Delta S_1$ (kcal/mol.K)
3:D4	2.64 ± 0.09	7.75 ± 1.70	−3.19 ± 0.01	1.43
neomycin:D4	0.94 ± 0.20	2.02 ± 0.20	−11.88 ± 0.32	−5.45
neomycin:D1	1.50 ± 0.04	3.80 ± 0.18	−6.89 ± 0.23	0.53

[a] Buffer conditions = 100 mM KCl, 10 mM SC, 0.5 mm EDTA, pH 6.8. T = 25 °C. [DNA] = 4 μM/duplex. [**3**] = 125 μM. [neomycin] = 250 μM.

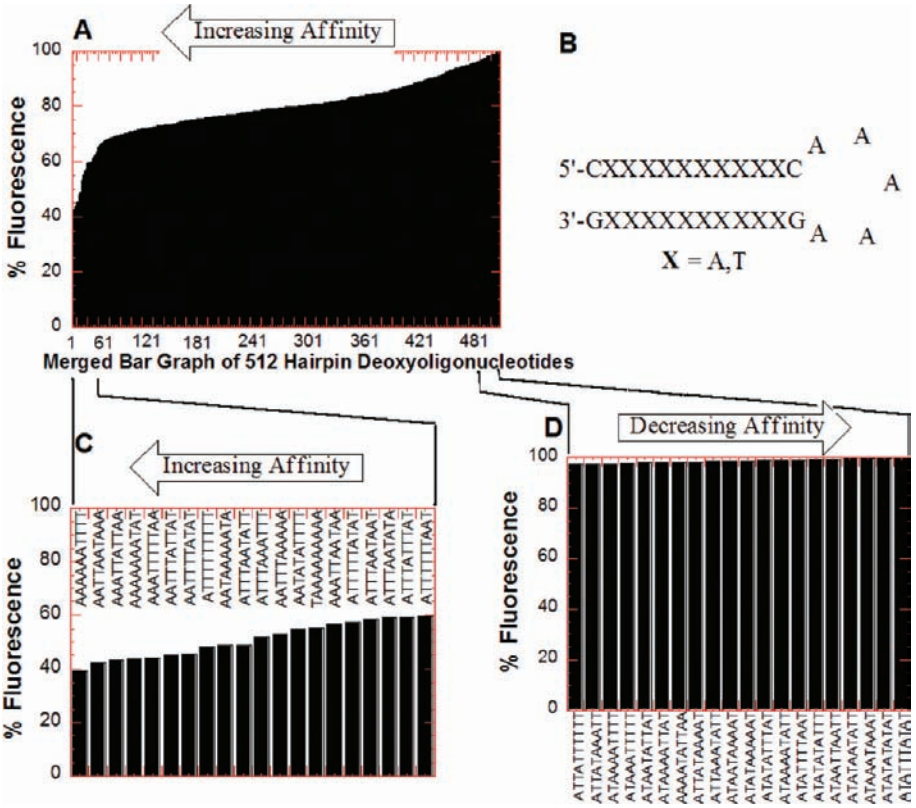

Figure 11. Results of the FID assay of **3** with 512 hairpin deoxyoligonucleotides. (A) Merged bar graph of 512 hairpin DNA oligonucleotides. (B) The common structure of hairpins. (C) Top 20 (highest affinity) hairpin sequences. (D) Bottom 20 (lowest affinity) hairpin sequences. After incubation at 25 °C for 30 min, each well was read (average of 10 readings) on a fluorescent plate reader (Ex. 495 nm, Em. 535 nm) in duplicate with two control wells (no ligand) 100% fluorescence, (no DNA) 0% fluorescence. Fluorescence readings are reported as percentage fluorescence relative to the control wells. Buffer conditions: 100 mM KCl, 10 mM SC, 0.5 mM EDTA, pH 6.8.

number of A to T switches (5′-ATATATATAT-3′, second to worst affinity hairpin). These results are consistent with the ITC-derived results that showed a much higher affinity of **3** toward continuous AT-rich sequences over alternating AT sequences. As found in our preliminary studies with the polynucleotides and designed deoxyoligonucleotides, alternating AT-rich duplexes show the lowest affinities (Figure 11D) whereas continuous stretches of AT tracts show the highest affinities (Figure 11C). We note that the aforementioned strong ten base pair binding site in sequence D3 (d[5′-G_3**A**$_5$**T**$_5$$C_3$-3′], Table 7) resides in the top 7% of the 512 sequences (see Supporting Information Table S2). The weakest ten base pair binding site resides in the sequence D9 (d[5′-G_3(**AT**)$_5$$C_3$-3′], Table 7), resides in the very bottom of the hairpin DNA library among the 512 sequences.

We then examined the probabilities of the A to T alternation in a subset of our hairpin library data. The "top 24" highest-affinity sequences have only 86 "switches" from A to T or vice versa (see Supporting Information Tables S2 and S3 for the list of sequences). If there was no correlation between sequence and affinity, we would expect 108 switches (24 × 9 × 0.5) in these 24 sequences. Compared to this null hypothesis, the probability that the 24 highest-affinity sequences would have 86 or fewer switches is 0.001%. Similarly, the "worst 24" lowest-affinity sequences have 125 "switches" from A to T or vice versa. If there was no correlation between sequence and affinity, we expect 108 switches (24 × 9 x 0.5) in these 24 sequences. Compared to this null hypothesis, the probability that the 24 lowest-affinity sequences would have 125 or more switches is 0.05%. The p values exceed 99% confidence levels ($p < 0.01$) for "top/bottom N" with any N value chosen, even $N = 1$. This analysis supports the claim that fewer A to T (or T to A) switches are correlated with a higher affinity of hairpin binding to dimer **3**.

Recognition of DNA Conformations: B* to B to A. The origin of the differences in binding sequence-specificity at the extremes can be broadly rationalized on the basis of the conformation

dx.doi.org/10.1021/ja108118v |*J. Am. Chem. Soc.* 2011, 133, 7361–7375

of DNA duplexes used in the study. AT-rich sequences adopt two conformations, canonical B-form and noncanonical B-form, depending upon the placement of AT bases. Previous reports have shown that AT-rich DNA homopolymers have more ordered hydration patterns and a non B-form conformation (some of these A-tract-containing sequences are referred to as B*),[54] when compared to more B-form alternating AT DNA duplexes.[72] This difference in hydration/structure is sufficient enough to affect thermodynamics of ligand binding to DNA.[72] For example, in previous studies where small molecule binders such as ethidium bromide (intercalator) and netropsin (groove binder) were studied as probes of DNA conformation, similar affinities were observed with drug binding to homopolymer poly(dA)·poly(dT) duplex as well as the alternating copolymer duplex poly(dA·dT)$_2$.[72] However, the enthalpy and entropy contributions to free energy were reversed in the two binding events. Due to the ordered hydration spheres, the A-tract sequences (continuous AT-rich sequences) tend to be more rigid structures; during the complexation of DNA with ligands, there is an expected melting of the hydration sphere of DNA. The melting causes the liberation of water molecules from DNA grooves to the bulk solution, resulting in a favorable entropy of binding. We observe a similar entropy driven binding for homopolymeric DNA (D3, Table 7) and a much more enthalpy driven binding toward the alternating DNA duplex (D9, Table 7). If the terminal G_3C_3 base pairs in D9 are replaced by alternating AT base pairs (D11, Table 7) to further disrupt the hydration, the thermodynamic signatures become completely enthalpy driven. However, as opposed to the enthalpy−entropy compensation commonly seen in the binding of minor groove binders and intercalators to duplex DNA,[72] DNA structure and hydration patterns lead to different affinities of **3** for these two types of DNA. Thus, while a complete thermodynamic analysis is necessary to use most DNA intercalators and minor groove binders as probes of DNA conformations, the carbohydrate-based ligands (dimer and monomer) identified here may represent a much simpler alternative as probes of B/B*- and A-form DNA conformations.

SUMMARY

We have used calorimetric and spectroscopic techniques to investigate the binding characterization of a newly synthesized carbohydrate ligand **3** with different nucleic acids. This ligand, in stark contrast to previously studied DNA binding ligands, is completely derived from nonaromatic aminosugar scaffolds. We have previously reported that aminosugars such as neomycin can act as a probe for A-form DNA. We have also explored aminoglycoside specificities by conjugating them with various nucleic acid binders. In this report, we have explored the binding of a dimeric aminoglycoside **3** with DNA duplexes and arrived at the following conclusions: (1) Dimer **3** has a clear preference toward AT-rich duplexes over GC-rich duplexes. (2) Dimer **3** has a large binding site (10−12 base pairs/ligand) and shows a clear preference for the AT-rich DNA duplex over a DNA triplex, as seen with oligonucleotides as well as polynucleotides, suggesting that the major groove is the likely binding site for **3**. (3) Binding affinity of **3** decreases with increasing salt concentration and shows that three ion pairs are involved in the binding of **3** with the DNA duplex. (4) Dimer **3** shows a preference for B and B*-DNA over A-form DNA, in stark contrast to the monomer neomycin, which prefers A-form DNA over B-form DNA. (5) Binding of **3** toward B*-DNA (nonalternating A-tract DNA duplexes) is favored by almost 50 fold over B-form DNA (alternating AT DNA) and almost 1000 fold over A-form DNA (GC-rich DNA).

The study outlines the first example of a major groove binding aminoglycoside-based ligand, in addition to being one of the first examples of a carbohydrate-only ligand that binds to A-tract DNA duplexes with such high affinity and shows a clear specificity toward nonalternating B*-form DNA duplexes. Additionally, few ligands that bind to such long stretches of DNA have ever been reported. Further work in this area with different carbohydrate-based scaffolds will extend the development of novel DNA duplex-specific carbohydrates to the recognition of mixed sequences with higher affinities and better specificities than with currently available DNA binders.

ASSOCIATED CONTENT

Supporting Information. Characterization data for **2**, **3a**, and **3**; experimental data for FID, CD, ITC, and UV thermal denaturation experiments. This material is available free of charge via the Internet at http://pubs.acs.org.

AUTHOR INFORMATION

Corresponding Author
dparya@clemson.edu

Present Addresses
[#]Department of Chemistry, University of the Pacific, Stockton, CA 95211.

ACKNOWLEDGMENT

This work was supported by NSF (CHE/MCB-0134932) and NIH (R15CA125724). We are thankful to Prof. Steve Stuart, Clemson University, for help with statistical analysis of the hairpin library binding data.

REFERENCES

(1) Dervan, P. B. *Bioorg. Med. Chem.* **2001**, *9*, 2215–2235.
(2) Hecht, S. M. *J. Am. Chem. Soc.* **2009**, *131*, 3791–3793.
(3) Neidle, S. In *The Molecular Basis for the Action of Some DNA-Binding Drugs*; Ellis, G. P., West, G. B., Eds.; ; Elsevier: New York, 1979; Vol. 16, pp 151−221.
(4) Long, E. C.; Barton, J. K. *Acc. Chem. Res.* **1990**, *23*, 271–273.
(5) Rao, K. E.; Lown, J. W. *Chem. Res. Toxicol.* **1991**, *4*, 661–669.
(6) Neidle, S. *Nat. Prod. Rep.* **2001**, *18*, 291–309.
(7) Wade, W. S.; Mrksich, M.; Dervan, P. B. *J. Am. Chem. Soc.* **1992**, *114*, 8783–8794.
(8) White, S.; Baird, E. E.; Dervan, P. B. *Biochemistry* **1996**, *35*, 12532–12537.
(9) Dervan, P. B. *Science* **1986**, *232*, 464–471.
(10) Dervan, P. B.; Burli, R. W. *Curr. Opin. Chem. Biol.* **1999**, *3*, 688–693.
(11) Willis, B.; Arya, D. P. *Curr. Org. Chem.* **2006**, *10*, 663–673.
(12) Ma, Q.; Akiyama, Y.; Xu, Z.; Konishi, K.; Hecht, S. M. *J. Am. Chem. Soc.* **2009**, *131*, 2013–2022.
(13) Animati, F.; Berettoni, M.; Bigioni, M.; Binaschi, M.; Felicetti, P.; Gontrani, L.; Incani, O.; Madami, A.; Monteagudo, E.; Olivieri, L.; Resta, S.; Rossi, C.; Cipollone, A. *ChemMedChem* **2008**, *3*, 266–279.
(14) Bross, P. F.; Beitz, J.; Chen, G.; Chen, X. H.; Duffy, E.; Kieffer, L.; Roy, S.; Sridhara, R.; Rahman, A.; Williams, G.; Pazdur, R. *Clin. Cancer Res.* **2001**, *7*, 1490–1496.

(15) Hayasaka, T.; Inoue, Y. *Biochemistry* **1969**, *8*, 2342–2347.
(16) Chapuis, J. C.; Schmaltz, R. M.; Tsosie, K. S.; Belohlavek, M.; Hecht, S. M. *J. Am. Chem. Soc.* **2009**, *131*, 2438–2439.
(17) Nicolaou, K. C.; Tsay, S. C.; Suzuki, T.; Joyce, G. F. *J. Am. Chem. Soc.* **1992**, *114*, 7555–7557.
(18) Bifulco, G.; Galeone, A.; Gomez-Paloma, L.; Nicolaou, K. C.; Chazin, W. J. *J. Am. Chem. Soc.* **1996**, *118*, 8817–8824.
(19) Bifulco, G.; Galeone, A.; Nicolaou, K. C.; Chazin, W. J.; Gomez-Paloma, L. *J. Am. Chem. Soc.* **1998**, *120*, 7183–7191.
(20) Schatz, A.; Bugie, E.; Waksman, S. A. *Proc. Soc. Exp. Biol. Med.* **1944**, *55*, 66–69.
(21) Waksman, S. A.; Lechevalier, H. A. *J. Antibiot.* **1949**, *109*, 305–309.
(22) Tok, J. B.; Cho, J.; Rando, R. R. *Biochemistry* **1999**, *38*, 199–206.
(23) Mei, H.; Galan, A. A.; Halim, N. S.; Mack, D. P.; Moreland, D. W.; Sanders, K. B.; Truong, H. N.; Czarnik, A. W. *Bioorg. Med. Chem. Lett.* **1995**, *5*, 2755–2760.
(24) Zapp, M. L.; Stern, S.; Green, M. R. *Cell* **1993**, *74*, 969–978.
(25) von Ahsen, U.; Davies, J.; Schroeder, R. *J. Mol. Biol.* **1992**, *226*, 935–941.
(26) Mikkelsen, N. E.; Brannvall, M.; Virtanen, A.; Kirsebom, L. A. *Proc. Natl. Acad. Sci. U.S.A.* **1999**, *96*, 6155–6160.
(27) Earnshaw, D. J.; Gait, M. J. *Nucleic Acids Res.* **1998**, *26*, 5551–5561.
(28) Tor, Y.; Hermann, T.; Westhof, E. *Chem. Biol.* **1998**, *5*, R277–83.
(29) Arya, D. P. *Acc. Chem. Res.* **2011**, *44*, 134–146.
(30) Thomas, J. R.; Hergenrother, P. J. *Chem. Rev.* **2008**, *108*, 1171–1224.
(31) Tor, Y. *Biochimie* **2006**, *88*, 1045–1051.
(32) Willis, B.; Arya, D. P. *Adv. Carbohydr. Chem. Biochem.* **2006**, *60*, 251–302.
(33) Arya, D. P. *Top. Curr. Chem.* **2005**, *253*, 149–178.
(34) Arya, D. P.; Micovic, L.; Charles, I.; Coffee, R. L., Jr.; Willis, B.; Xue, L. *J. Am. Chem. Soc.* **2003**, *125*, 3733–3744.
(35) Arya, D. P.; Coffee, R. L., Jr.; Willis, B.; Abramovitch, A. I. *J. Am. Chem. Soc.* **2001**, *123* (23), 5385–5395.
(36) Arya, D. P.; Coffee, R. L., Jr.; Charles, I. *J. Am. Chem. Soc.* **2001**, *123*, 11093–11094.
(37) Arya, D. P.; Coffee, R. L., Jr. *Bioorg. Med. Chem. Lett.* **2000**, *10*, 1897–1899.
(38) Xi, H.; Arya, D. P. *Curr. Med. Chem. Anticancer Agents* **2005**, *5*, 327–338.
(39) Shaw, N. N.; Arya, D. P. *Biochimie* **2008**, *90*, 1026–1039.
(40) Shaw, N. N.; Xi, H.; Arya, D. P. *Bioorg. Med. Chem. Lett.* **2008**, *18*, 4142–4145.
(41) Xi, H.; Gray, D.; Kumar, S.; Arya, D. P. *FEBS Lett.* **2009**, *583*, 2269–2275.
(42) Ranjan, N.; Andreasen, K. F.; Kumar, S.; Hyde-Volpe, D.; Arya, D. P. *Biochemistry* **2010**, *49*, 9891–9903.
(43) Xue, L.; Xi, H.; Kumar, S.; Gray, D.; Davis, E.; Hamilton, P.; Skriba, M.; Arya, D. P. *Biochemistry* **2010**, *49*, 5540–5552.
(44) Willis, B.; Arya, D. P. *Biochemistry* **2006**, *45*, 10217–10232.
(45) Arya, D. P.; Willis, B. *J. Am. Chem. Soc.* **2003**, *125*, 12398–12399.
(46) Willis, B.; Arya, D. P. *Bioorg. Med. Chem. Lett.* **2009**, *19*, 4974–4979.
(47) Charles, I.; Xi, H.; Arya, D. P. *Bioconjugate Chem.* **2007**, *18*, 160–169.
(48) Charles, I.; Xue, L.; Arya, D. P. *Bioorg. Med. Chem. Lett.* **2002**, *12*, 1259–1262.
(49) Charles, I.; Arya, D. P. *J. Carbohydr. Chem.* **2005**, *24* 145–160.
(50) Napoli, S.; Carbone, G. M.; Catapano, C. V.; Shaw, N.; Arya, D. P. *Bioorg. Med. Chem. Lett.* **2005**, *15*, 3467–3469.
(51) Arya, D. P.; Xue, L.; Willis, B. *J. Am. Chem. Soc.* **2003**, *125* (34), 10148–10149.
(52) Michael, K.; Wang, H.; Tor, Y. *Bioorg. Med. Chem.* **1999**, *7*, 1361–1371.
(53) Arya, D. P.; Coffee, R. L., Jr.; Xue, L. *Bioorg. Med. Chem. Lett.* **2004**, *14*, 4643–4646.
(54) Hud, N. V.; Plavec, J. *Biopolymers* **2003**, *69*, 144–158.
(55) Wang, H.; Tor, Y. *Bioorg. Med. Chem. Lett.* **1997**, *7*, 1951–1956.
(56) Ryu, D. H.; Litovchick, A.; Rando, R. R. *Biochemistry* **2002**, *41*, 10499–10509.
(57) Willis, B.; Arya, D. P. *Biochemistry* **2010**, *49*, 452–469.
(58) Kirk, S. R.; Luedtke, N. W.; Tor, Y. *J. Am. Chem. Soc.* **2000**, *122*, 980–981.
(59) Benveniste, R.; Davies, J. *Antimicrob. Agents Chemother.* **1973**, *4*, 402–409.
(60) Liu, X.; Thomas, J. R.; Hergenrother, P. J. *J. Am. Chem. Soc.* **2004**, *126*, 9196–9197.
(61) Agnelli, F.; Sucheck, S. J.; Marby, K. A.; Rabuka, D.; Yao, S.; Sears, P. S.; Liang, F.; Wong, C. *Angew. Chem., Int. Ed.* **2004**, *43*, 1562–1566.
(62) Tok, J. B.; Dunn, L. J.; Des Jean, R. C. *Bioorg. Med. Chem. Lett.* **2001**, *11*, 1127–1131.
(63) Greenberg, W. A.; Priestley, E. S.; Sears, P. S.; Alper, P. B.; Rosenbohm, C.; Hendrix, M.; Hung, S.; Wong, C. *J. Am. Chem. Soc.* **1999**, *121*, 6527–6541.
(64) Boger, D. L.; Fink, B. E.; Brunette, S. R.; Tse, W. C.; Hedrick, M. P. *J. Am. Chem. Soc.* **2001**, *123*, 5878–5891.
(65) Xi, H.; Kumar, S.; Dosen-Micovic, L.; Arya, D. P. *Biochimie* **2010**, *92*, 514–529.
(66) Record, M. T., Jr; Anderson, C. F.; Lohman, T. M. *Q. Rev. Biophys.* **1978**, *11*, 103–178.
(67) Gray, D. M.; Ratliff, R. L.; Vaughan, M. R. *Methods Enzymol.* **1992**, *211*, 389–406.
(68) Ivanov, V. I.; Minchenkova, L. E.; Schyolkina, A. K.; Poletayev, A. I. *Biopolymers* **1973**, *12*, 89–110.
(69) Tse, W. C.; Boger, D. L. *Acc. Chem. Res.* **2004**, *37*, 61–69.
(70) Yeung, B. K. S.; Tse, W. C.; Boger, D. L. *Bioorg. Med. Chem. Lett.* **2003**, *13*, 3801–3804.
(71) Monchaud, D.; Allain, C.; Teulade-Fichou, M. *Bioorg. Med. Chem. Lett.* **2006**, *16*, 4842–4845.
(72) Breslauer, K. J.; Remeta, D. P.; Chou, W. Y.; Ferrante, R.; Curry, J.; Zaunczkowski, D.; Snyder, J. G.; Marky, L. A. *Proc. Natl. Acad. Sci. U.S.A.* **1987**, *84*, 8922–8926.